UNIVERSITY OF CALIFORNIA, SAN DIEGO

Fat-Resident Regulatory T Cells Drive Age-Associated Insulin Resistance

A dissertation submitted in partial satisfaction of the requirements for the degree Doctor of Philosophy

in

Biomedical Sciences

by

Sagar Pradeep Bapat

Committee in charge:

Professor Ye Zheng, Chair
Professor Christopher K. Glass, Co-Chair
Professor John T. Chang
Professor Don W. Cleveland
Professor Ronald M. Evans
Professor Richard L. Gallo
Professor Anjana Rao

2016

The Dissertation of Sagar Pradeep Bapat is approved, and it is acceptable in quality and form for publication on microfilm and electronically:

_____

_____

_____

_____

_____

_____
Co-Chair

_____
Chair

University of California, San Diego

2016

DEDICATION

To my Teachers — past, present, and future.

EPIGRAPH

Our greatest responsibility is to be good ancestors.

Jonas Salk

TABLE OF CONTENTS

LIST OF FIGURES

LIST OF TABLES

ACKNOWLEDGEMENTS

The contents and data presented in this dissertation is adapted from a Letter which was published in 2015 in the journal *Nature* titled “Depletion of fat-resident Treg cells prevents age-associated insulin resistance.” The authorship of this Letter is: Sagar P. Bapat, Jae Myoung Suh, Sungsoon Fang, Sihao Liu, Yang Zhang, Albert Cheng, Carmen Zhou, Yuqiong Liang, Mathias LeBlanc, Christopher Liddle, Annette R. Atkins, Ruth T. Yu, Michael Downes, Ronald M. Evans and Ye Zheng.

I am supported by National Institutes of Health (NIH) grants (DK096828 and T32 GM007198). Christopher Liddle and Michael Downes are funded by grants from the National Health and Medical Research Council of Australia Project Grants 512354, 632886 and 1043199. Ronald M. Evans is an Investigator of the Howard Hughes Medical Institute (HHMI) at the Salk Institute and March of Dimes Chair in Molecular and Developmental Biology, and is supported by National Institutes of Health (NIH) grants (DK057978, DK090962, HL088093, HL105278 and ES010337), the Glenn Foundation for Medical Research, the Leona M. and Harry B. Helmsley Charitable Trust, Ipsen/Biomeasure, California Institute for Regenerative Medicine and The Ellison Medical Foundation. Ye Zheng is supported by the Nomis Foundation, the Rita Allen Foundation, the Emerald Foundation, the Hearst Foundation, the National Multiple Sclerosis Society, and National Institute of Health (AI099295, AI107027). This work was also supported by National Cancer

Institute funded Salk Institute Cancer Center core facilities (CA014195) and the James B. Pendleton Charitable Trust.

VITA

2005-2009	Leland Stanford Junior University Bachelor of Science, Chemistry
2009-2011	University of California, San Diego, School of Medicine Medical Scientist Training Program, Years 1-2 Medical Student
2011-2015	University of California, San Diego, School of Medicine Medical Scientist Training Program, Years 3-6 Biomedical Sciences Graduate Student
2011-2015	The Salk Institute for Biological Studies Nomis Foundation Laboratories for Immunobiology and Microbial Pathogenesis Gene Expression Laboratory Graduate Research
2016	University of California, San Diego Doctor of Philosophy, Biomedical Sciences
2015-2017	University of California, San Diego, School of Medicine Medical Scientist Training Program, Years 7-8 Medical Student

ABSTRACT OF THE DISSERTATION

Fat-Resident Regulatory T Cells Drive Age-Associated Insulin Resistance

by

Sagar Pradeep Bapat

Doctor of Philosophy in Biomedical Sciences

University of California, San Diego, 2016

Professor Ye Zheng, Chair
Professor Christopher K. Glass, Co-Chair

Age-associated insulin resistance (IR) and obesity-associated IR are two physiologically distinct forms of adult onset diabetes. While macrophage-driven inflammation is a core driver of obesity-associated IR[1-6], the underlying mechanisms of the obesity-independent yet highly prevalent age-associated

IR[7] are largely unexplored. Comparative adipo-immune profiling (AIP) reveals that fat-resident regulatory T cells, termed fTregs, progressively accumulate in adipose tissue as a function of age, but not obesity. Supporting the existence of two distinct mechanisms underlying age-associated versus obesity-associated IR, mice deficient in fTregs are protected against age-associated IR, yet remain susceptible to obesity-associated IR and metabolic disease. In contrast, selective depletion of fTregs via anti-ST2 antibody treatment increases adipose tissue insulin sensitivity. These findings establish that distinct immune cell populations within adipose tissue underlie aging- and obesity-associated IR and implicate fTregs as adipo-immune drivers and potential therapeutic targets in the treatment of age-associated IR.

CHAPTER 1: INTRODUCTION TO THE MAIN TEXT

TAKING INSPIRATION FROM THE IMMUNOMETABOLIC PARADIGM OF OBESITY-ASSOCIATED INSULIN RESISTANCE

Type-2 diabetes is an ever-growing epidemic in the modern world whose associated co-morbidity and mortality represent an enormous human disease burden on an individual and socioeconomic level. As of 2014, 29.1 million people are estimated to have diabetes and another 86 million people are estimated to have prediabetes in the United States alone. The total medical costs and lost work and wages of people who are positively diagnosed with diabetes in 2014 was $245 billion, though the actual cost will be higher if the associated economic costs from undiagnosed diabetics are included[7]. The range of co-morbidities associated with type-2 diabetes includes blindness, kidney failure, heart failure, stroke, and amputations of toes, feet, and legs, all of which impose tremendous burdens on the diabetic patient, his or her immediate caretakers, and the healthcare system as a whole.

Type-2 diabetes is the clinical manifestation of systemic insulin resistance and a consequent inability to maintain glucose homeostasis. Insulin resistance has two chief etiologies - obesity and aging. However, the current clinical management options of patients with type-2 diabetes focus almost exclusively on ameliorating obesity-associated insulin resistance with little regard to the possibility that the presenting patient's insulin resistance could be secondary to advancing age and not increased body mass index (BMI). In fact, many of the lifestyle/behavior modifications and pharmacological interventions offered do not change for a patient with a BMI of 32 (clinically obese) or 23 (normal), focusing ultimately on losing weight, increasing

exercise, and modulating target organ insulin sensitivity or pancreatic insulin secretion. While many pharmacological interventions and even lifestyle/ behavior modifications have been proven effective - two large studies in Finland[8] and the United States[9] documented a ~50% decrease in the risk of prediabetics progressing to type-2 diabetes upon a decrease of ~4 kg in weight due to behavior modification - a key problem remains: long-term effectiveness remains a challenge as disease progression is largely inevitable with time[10-12]. In fact, a recent study found that clinically well-managed type-2 diabetes still decreases the life expectancy of a 55 year old male by an average of ~3 years[13], indicating that medical treatment still does not provide satisfactory health outcomes. Clearly, the clinician is in need of new tools to more effectively help patients better manage type-2 diabetes, and as humans live longer and longer into the ninth decade and beyond, aging-associated insulin resistance must be considered as a possible etiology of any presenting patient's diabetes.

While obesity-associated insulin resistance has been the subject of intense scientific investigation by many scientists in academia and the biotechnology industry, there has been much less research and insight into how aging-associated insulin resistance occurs. Because of this, we sought to understand how progressive aging increases the risk for diabetes, independent of obesity. As a starting point, we looked at the abundance of literature that has shed light on how the setting of obesity promotes insulin

resistance. While several physiological, cellular, and molecular pathways have been elucidated toward this end, one consensus process has emerged as linking obesity to insulin resistance - chronic inflammation.

A series of landmark studies over the last 25 years have shown definitively in mice that obesity, either induced by providing a high fat diet or through genetic means, elicits inflammatory machinery composed of cytokines and immune cells that persists chronically in the obese state and progressively induces an insulin-resistant phenotype. Of note, the inflammatory cytokine tumor necrosis factor alpha (TNFa) was shown to have increased expression in adipose tissue of obese mice compared with lean mice, and blunting of TNFa signaling in adipose tissue was shown to protect against obesity-associated insulin resistance[14-16]. Furthermore, the increased TNFa cytokine expression was also coupled with increased macrophage content within obese adipose tissue, and these adipose tissue macrophages (ATMs) were shown to be the chief source of the obesity-associated TNFa increase. Additional studies showed that abrogating ATM content or ATM inflammatory signaling pathways alleviated obesity-associated insulin resistance in mice[5,18-19]. These foundational studies, along with thousands of other studies, showed unequivocally that the increased systemic and local inflammatory tone secondary to obesity was a driver of insulin resistance.

Leveraging this well-established immuno-metabolic paradigm for obesity-associated insulin resistance in the mouse - whereby obesity increases

adipose tissue macrophage content, increasing inflammatory cytokine secretion and enforcing a state of chronic inflammation and insulin resistance - we sought to ask if a similar immune-metabolic pathway exists in aging-associated insulin resistance. Is there a immune cell type that is preferentially increased in aged adipose tissue? If so, does that immune cell type drive aging-associated insulin resistance? The following text provides evidence that this is in fact the case in mouse.

CHAPTER 2: MAIN TEXT OF THE DISSERTATION

FAT-RESIDENT REGULATORY T CELLS DRIVE AGE-ASSOCIATED INSULIN RESISTANCE

Age-associated insulin resistance (IR) and obesity-associated IR are two physiologically distinct forms of adult onset diabetes. While macrophage-driven inflammation is a core driver of obesity-associated IR[1-6], the underlying mechanisms of the obesity-independent yet highly prevalent age-associated IR[7] are largely unexplored. Comparative adipo-immune profiling (AIP) reveals that fat-resident regulatory T cells, termed fTregs, progressively accumulate in adipose tissue as a function of age, but not obesity. Supporting the existence of two distinct mechanisms underlying age-associated versus obesity-associated IR, mice deficient in fTregs are protected against age-associated IR, yet remain susceptible to obesity-associated IR and metabolic disease. In contrast, selective depletion of fTregs via anti-ST2 antibody treatment increases adipose tissue insulin sensitivity. These findings establish that distinct immune cell populations within adipose tissue underlie aging- and obesity-associated IR and implicate fTregs as adipo-immune drivers and potential therapeutic targets in the treatment of age-associated IR.

The young, lean state is associated with insulin sensitivity, however both aging and obesity can lead to the development of insulin resistance (IR, Fig. 1a). To distinguish key immune cell types that drive age- versus obesity-associated IR, we quantitatively profiled the immune cell components of adipose depots using a flow cytometry approach termed adipo-immune profiling (AIP) (Fig. 2a-c, Table 1). In contrast to the decrease in anti-inflammatory M2 adipose tissue macrophages (ATMs) and eosinophils

observed in obesity-driven IR, AIP revealed that these cell populations are largely unperturbed in visceral adipose tissue (VAT) from aged mice (M2 ATMs – aged: 33.6 ± 3.8%, young: 29.8 ± 4.1%, obese: 22.9 ± 6.3%; eosinophils – aged: 4.4% ± 1.6%, young: 4.7% ± 0.7%, obese: 0.8% ± 1.0%, Fig. 1b)[20-24]. Rather, the relative portion of the non-macrophage compartment is significantly increased in aged compared to young or obese mice (aged: 24.3 ± 4.6%, young: 17.9 ± 2.8%, obese 15.7 ± 3.8%, Fig. 1b), which is largely attributable to a ~13.5 fold expansion in the fat-resident regulatory T cell (fTreg) population (aged: 5.0 ± 1.2%, young: 0.4 ± 0.1%, obese: 0.1 ±0.1%, Fig. 1b, c)[25,26]. These varying AIP signatures of adipose tissue suggest that distinct pathophysiologic processes drive age- and obesity-associated IR and implicate fTregs as potential drivers of age-associated IR.

To explore the role of fTregs in age-associated IR, we utilized *Foxp3*^{Cre} *Pparγ*$^{fl/fl}$ mice in which Tregs are selectively depleted from VAT (fTreg KO mice, Fig. 3a, Fig. 4)[27] without significantly altering the immune profiles of subcutaneous adipose tissue (SAT) or spleen (Fig. 5a,b). Importantly, the VAT-specific loss of fTregs does not elicit any overt signs of systemic inflammation generally associated with Treg dysfunction. Aged fTreg KO mice have normal-sized spleens and increased CD62L^{hi} CD44^{lo} naive CD4^{+} T cell populations compared to WT controls (Fig. 3c, Fig. 6a). The normal intestinal histology provides additional evidence that the Treg population is not perturbed (Fig. 6b,c). Furthermore, no differences are observed in the levels of inflammatory

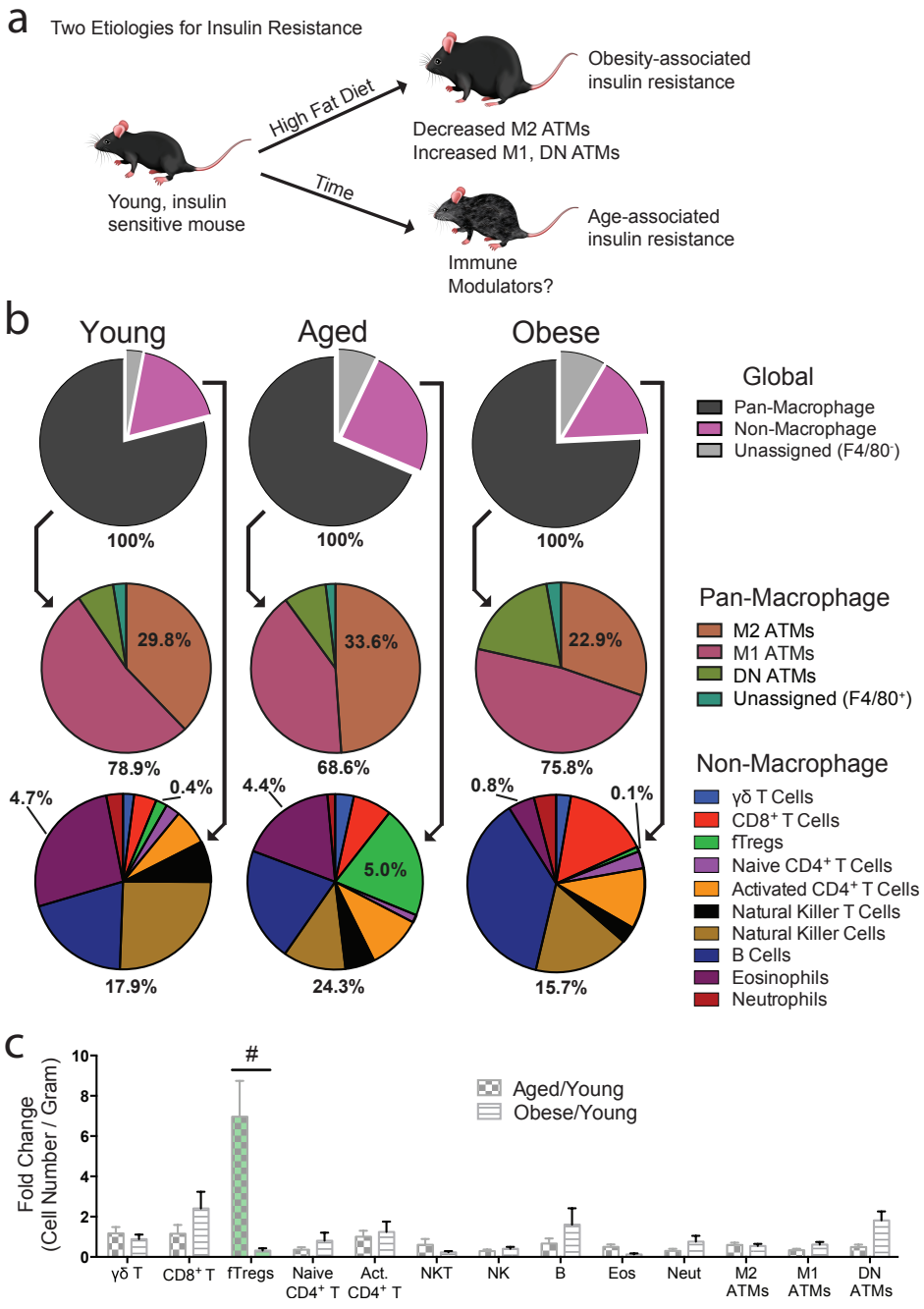

Figure 1. fTregs are selectively enriched in aged mice. (**a**) Schematic outlining study premise. (**b**) Visceral adipose tissue (VAT) Adipo-immune profiles (AIP) from mice at 12 weeks (young, n=10), 44 weeks (aged, n=10), and in diet-induced obese (DIO) mice (n=10). Immune cells abundance, expressed as percentage of CD45.2+ cells. (**c**) Changes in immune cell abundance between indicated groups, expressed as fold change in cell number per gram of VAT. #, false discovery rate < 2%. Obese mice were fed a high fat diet for 12 weeks from 12 weeks of age. Data represents mean ± s.e.m.

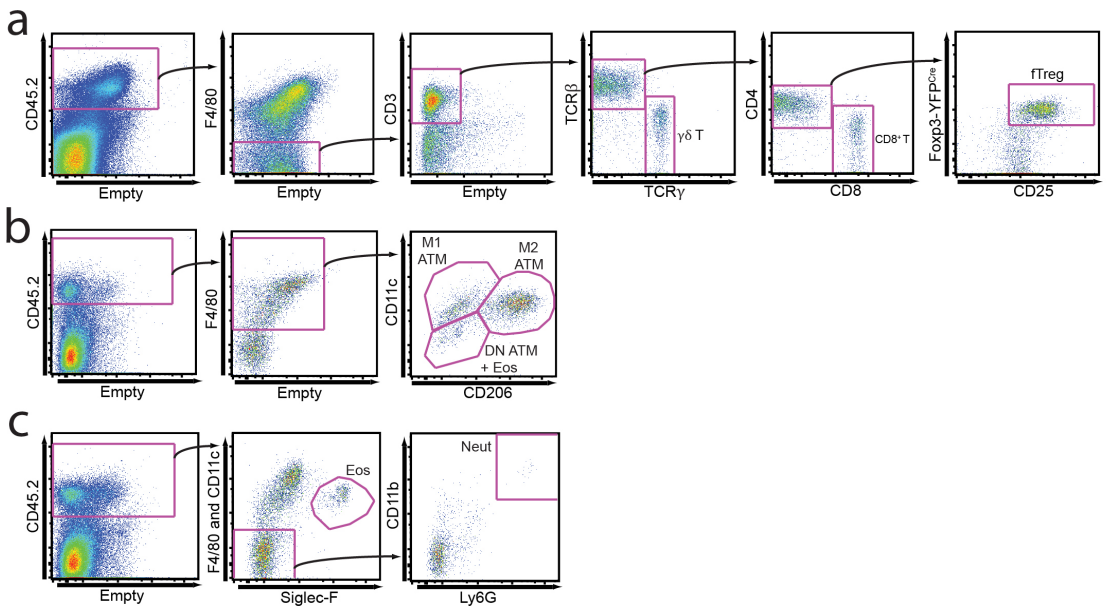

Figure 2. Selected gating strategies used to generate AdipoImmune Profiles. AdipoImmune Profiles were generated through the use of several distinct antibody cocktails. (**a-c**) Here using Foxp3$^{Cre\text{-}YFP}$ reporter mice we show how the stromal vascular fraction of VAT was analyzed by flow cytometry to identify several T cell subtypes (**a**), macrophage subsets (**b**), and eosinophils and neutrophils (**c**).

Table 1. Table outlining the antibodies used to molecularly identify the given immune cell type.

Immune Cell Type	Molecular Identification Scheme
TCRγδ	CD45.2^{+} F4/80^{-} CD3^{+} TCRb^{-} TCRγ^{+}
CD8^{+}	CD45.2^{+} F4/80^{-} CD3^{+} TCRb^{+} CD4^{-} CD8^{+}
Treg CD4^{+}	CD45.2^{+} CD4^{+} CD25^{+} Foxp3^{+}
Naive CD4^{+}	CD45.2^{+} CD4^{+} CD25^{-} Foxp3^{-} CD62L^{hi} CD44^{lo}
Activated CD4^{+}	CD45.2^{+} CD4^{+} CD25^{-} Foxp3^{-} CD62L^{lo} CD44^{hi}
NKT	CD45.2^{+} NK1.1^{+} TCRb^{+}
NK	CD45.2^{+} NK1.1^{+} TCRb^{-}
B	CD45.2^{+} NK1.1^{-} CD19^{+}
Eosinophil	CD45.2^{+} F4/80^{+} Siglec-F^{+}
Neutrophil	CD45.2^{+} F4/80^{-} CD11c- CD11b^{+} Ly6G^{+}
M2 ATM	CD45.2^{+} F4/80^{+} CD11c^{med} CD206^{+}
M1 ATM	CD45.2^{+} F4/80^{+} CD11c^{hi} CD206^{-}
DN (Double-negative) ATM	CD45.2^{+} F4/80^{+} CD11c^{-} CD206^{-}

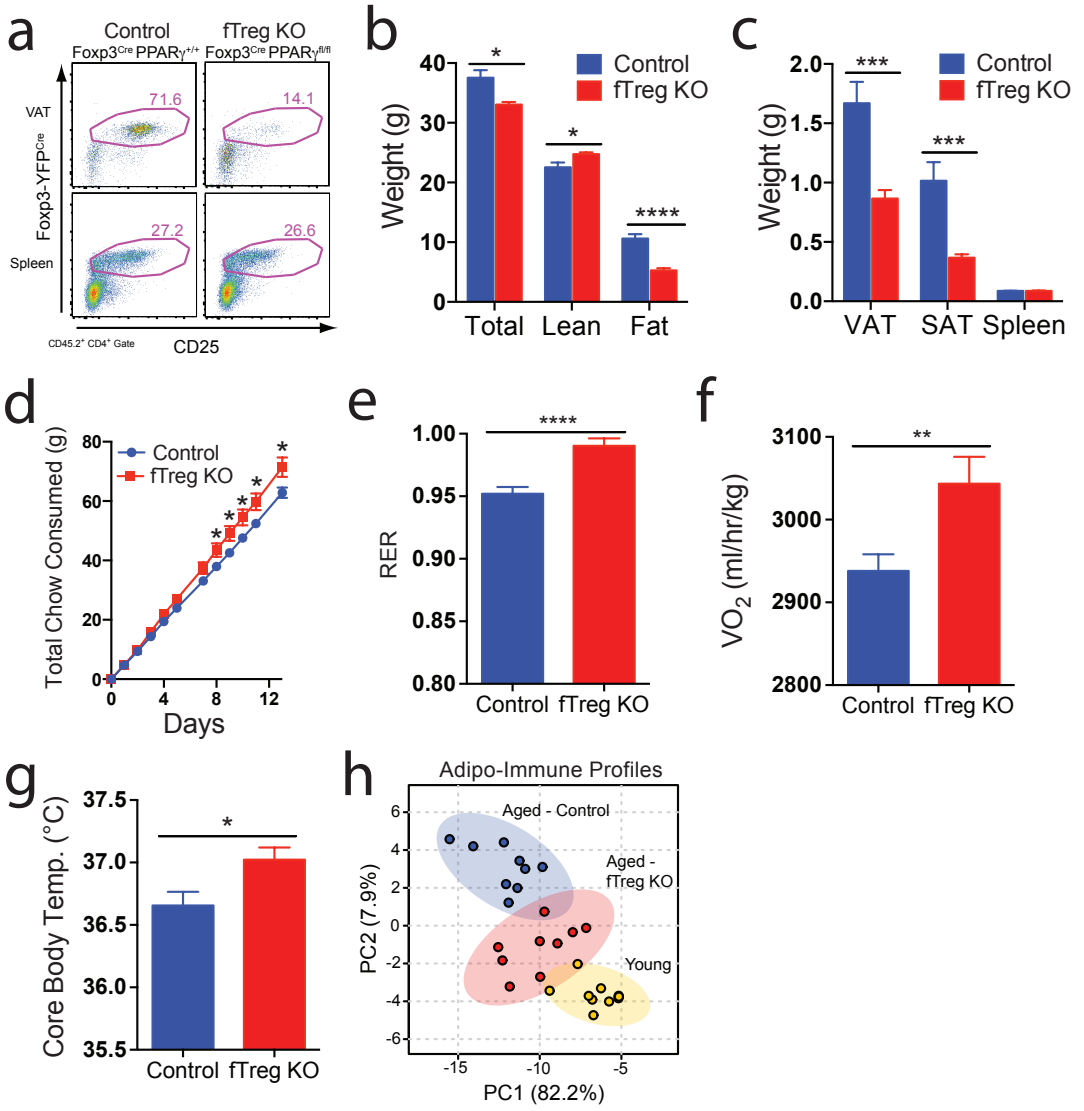

Figure 3. fTreg KO mice are protected from general hallmarks of metabolic aging. (**a**) Representative FACS plots of fTreg KO (Foxp3^{Cre} PPAR$\gamma^{fl/fl}$) and control (Foxp3^{Cre} PPAR$\gamma^{+/+}$) mice depicting Treg enrichment in VAT and spleen. **(b)** Total body weight (n=15 per group), and lean and fat mass of control and fTreg KO mice (~12 months, n=8 per group). (**c**) Mass of VAT, SAT, and spleen in aged control and fTreg KO mice (~15 months, n=9 per group). (**d**) Cumulative food consumption of control and fTreg KO mice (~8-9 months old, n=8 per group). (**e-f**) Average 24 hour respiratory exchange ratio (RER) of (**e**) and average VO_2 consumed by (**f**) aged control and fTreg KO mice (~11 months, n=6 per group) (**g**) Core body temperature of control and fTreg mice (~13 months old, n=9 per group). (**h**) Principal component analysis of non-macrophage AIPs of young (12 weeks), aged (~15 months) and aged-fTreg KO (~15 months) mice. Data represents mean ± s.e.m. *p<0.05, **p<0.01, ***p<0.001, ****p<0.0001.

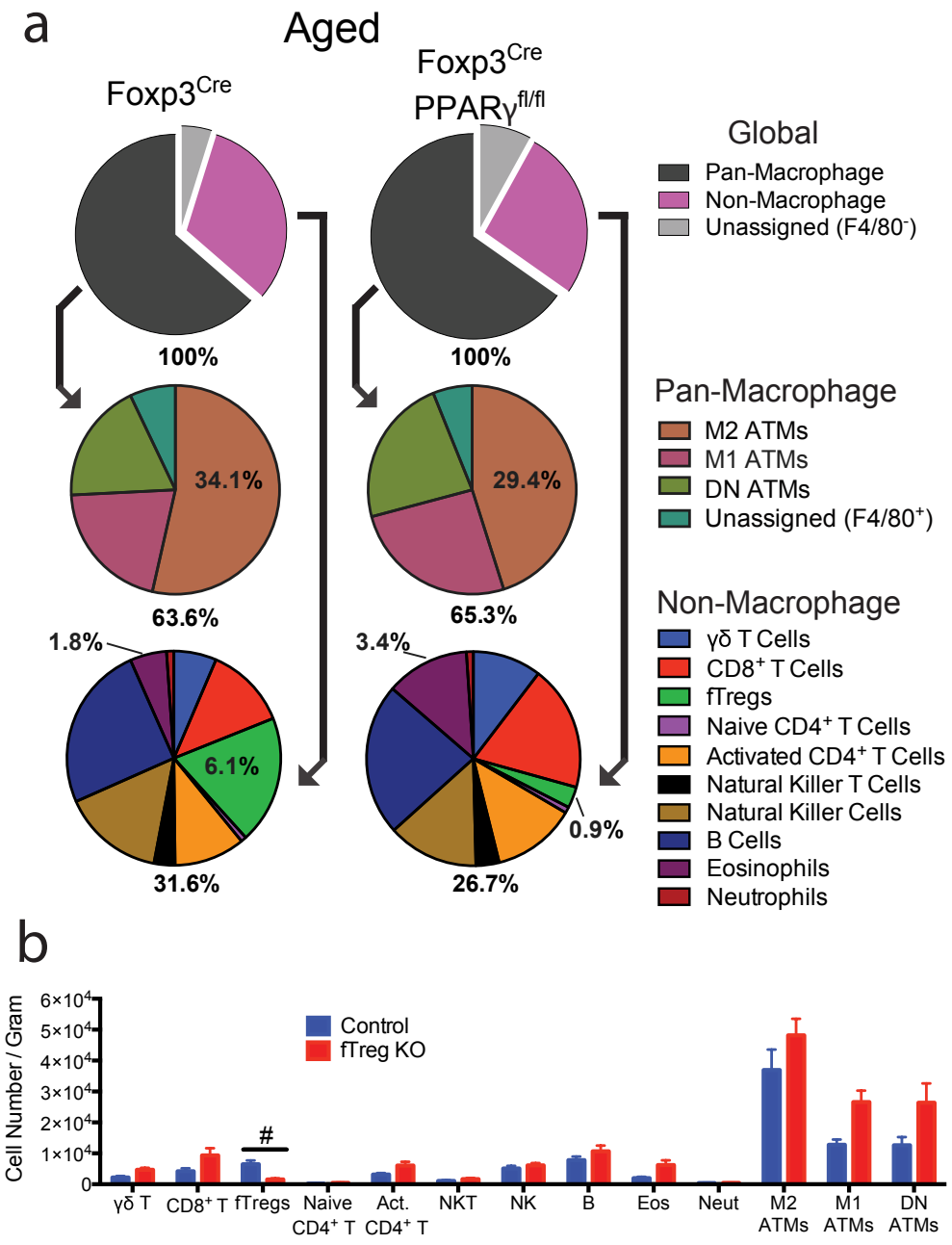

Figure 4. VAT AdipoImmune profiles of aged fTreg KO and control mice. (**a**) AdipoImmune profiles of aged (~14 months old) fTreg KO and control mice male mice depicting immune cell abundance, expressed as percentag13e of CD45.2+ cells. Entirety of immune compartment (top) is further divided into pan-macrophage (middle) and non-macrophage (bottom) pie charts (n=9 mice per group). (**b**) Immune cell abundance between fTreg KO and control mice, expressed as cells per gram of VAT (n=9 mice per group). #, false discovery rate < 2%. Data represents mean ± s.e.m.

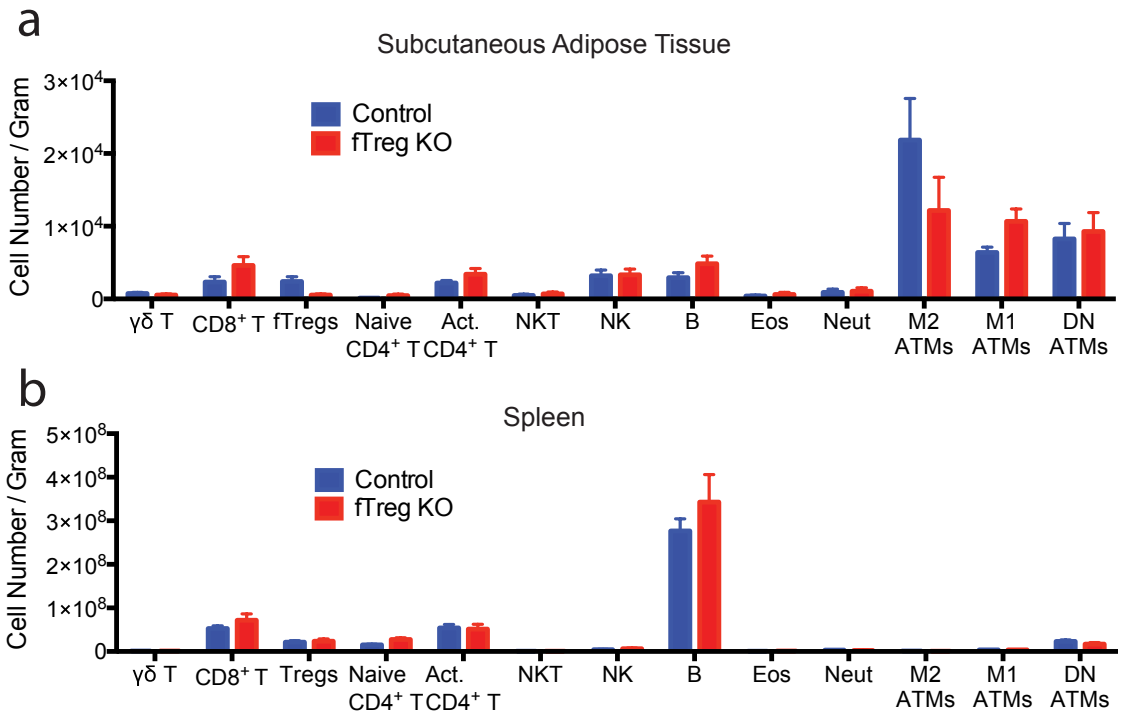

Figure 5. SAT AdipoImmune and spleen immune profiles of fTreg KO and control mice. (**a-b**) Immune cell abundance between fTreg KO and control mice, expressed as cells per gram of SAT (**a**) and spleen (**b**) (n=9 mice per group). Data represents mean ± s.e.m.

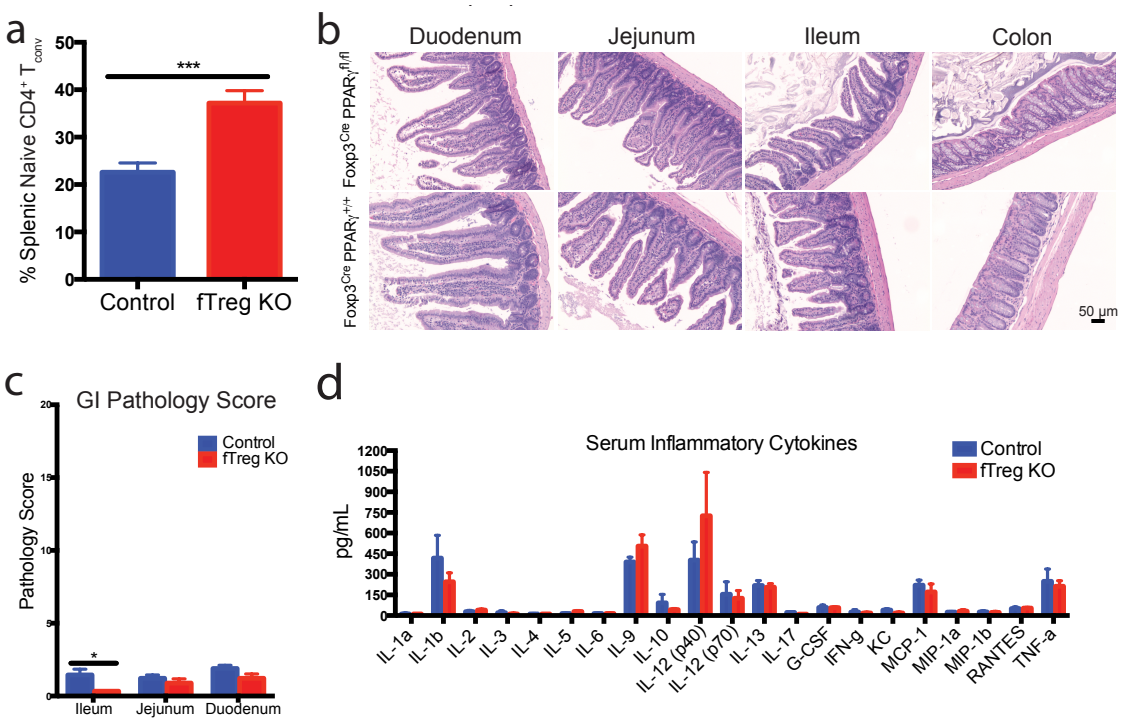

Figure 6. Aged fTreg KO mice do not show signs of systemic autoimmunity or breakdown in peripheral tolerance. (**a**) Percentage of splenic naive CD4+ T cells as defined by CD62hi CD44lo relative to total CD4+ Foxp3-YFP- CD25- population (n=9 mice per group). (**b**) Representative histology of gastrointestinal tract — duodenum, jejunum, ileum, colon (left to right). (n=3 mice per group). There were no significant lesions observed or differences in inflammation, epithelial changes, or mucosal architecture between the two groups (H&E, x100, scale bar 50 [?]m). (**c**) Histopathology score in the small intestine and colon of fTreg KO and control mice. The severity and extent of inflammation and epithelial changes as well as mucosal architecture were each graded on a score of 1 (minimal) to 5 (severe) and added to obtain an overall score over 20. There were minimal inflammatory changes with no significant differences between groups. (**d**) Multiplex inflammation panel of serum from fTreg KO and control mice (n=4 pooled samples (3 mice per sample) per group).

cytokines, including TNFα, IL1β, IL6, IFNγ, and IL17, in the serum of aged fTreg KO compared to control mice (Fig. 6d).

Intriguingly, the selective loss of fTregs attenuates many of the hallmarks of age-associated metabolic dysregulation[28]. They weigh less than control mice and are leaner (decreased VAT and SAT adiposity) despite increased food consumption (Fig. 3b,c,d). In addition, the respiratory exchange ratio (RER, Fig. 3e), oxygen consumption (Fig. 3f), and core body temperature (Fig. 3g) are increased in aged fTreg KO mice relative to control mice. These marked improvements suggest that the age-associated metabolic phenotype is closely linked with VAT immune responses, and that in the aged setting, a reduction in fTreg numbers may be protective. Indeed, the AIPs of aged fTreg KO mice are shifted towards those of young mice, as visualized by principal component analysis (Fig. 3h).

The fTreg KO phenotype is most pronounced in aged mice, though a reduction in fTreg levels is also seen in obese fTreg KO mice (Fig. 7a). Consistent with the notion that fTregs are drivers of age-associated metabolic dysregulation, fasting serum glucose and insulin levels are significantly reduced in aged fTreg KO mice (Fig. 7b,c, Fig. 8). Furthermore, aged fTreg KO mice display smaller glucose excursions during glucose tolerance tests and increased sensitivity during insulin tolerance tests compared to weight-matched control mice (Fig. 7e). Notably, these improvements in glucose homeostasis are observed only in aged mice; no significant differences are

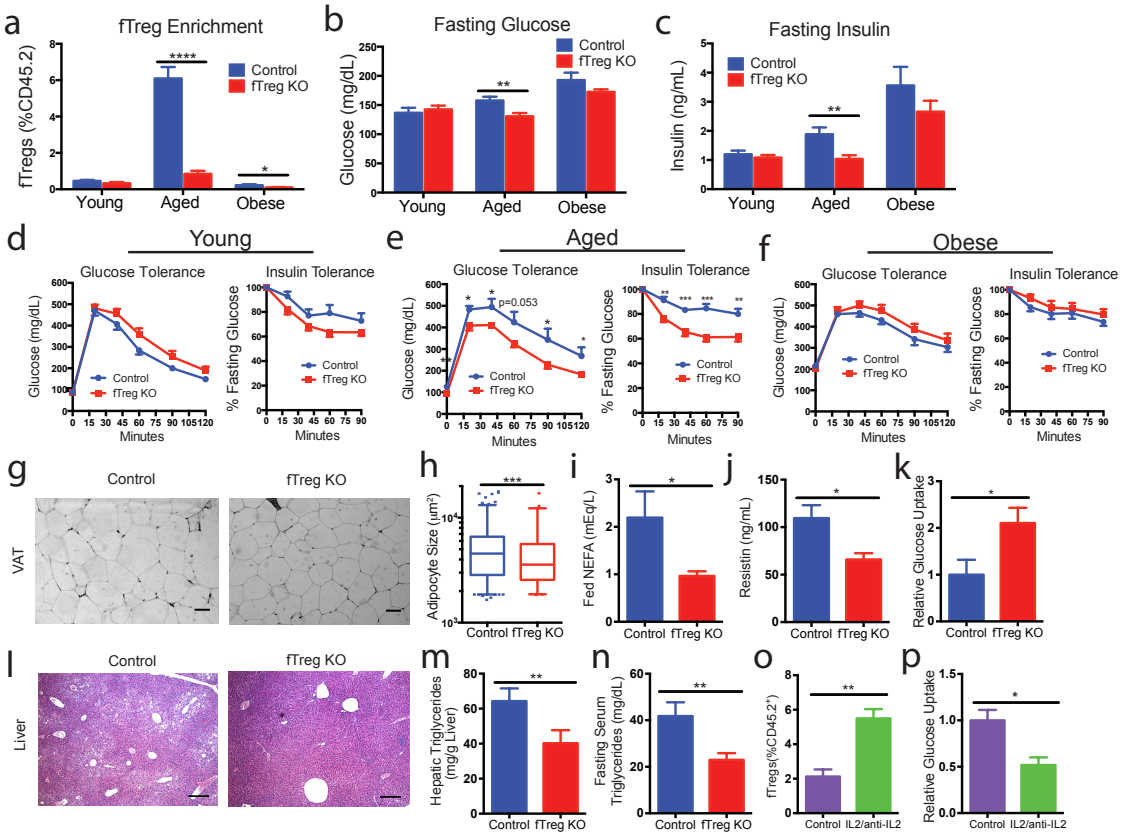

Figure 7. Loss of fTregs protects against the clinical hallmarks of age-associated 8insulin resistance. (**a**) fTreg levels in VAT from control and fTreg KO ($Foxp3^{Cre}$ $PPAR\gamma^{fl/fl}$) mice in young (control n=6; fTreg KO n=6), aged (~15 months old; control n=10; fTreg KO n=10), and obese mice (control n=6; fTreg KO n=8). (**b**) Fasting serum glucose and (**c**) insulin levels in control and fTreg KO mice in young (control n=9; fTreg KO n=9), aged (36 weeks old, control n=9; fTreg KO n=11), and obese mice (control n=10; fTreg KO n=10). Glucose tolerance and insulin tolerance tests of control and fTreg KO mice at **(d)** young (12 weeks, control n=8; fTreg KO n=8), (**e**) aged (36-37 weeks, control n=8; fTreg KO n=9), and (**f**) obese mice (control n=9; fTreg KO n=10). (**g**) Representative H&E staining of visceral adipose tissue (VAT, gonadal) from ~14 month old control (n=3) and fTreg KO mice (n=5) (scale bar, 50 μM). (**h**) Box and whisker plot of adipocyte size distribution in visceral adipose tissue from control (n=3) and fTreg KO mice (n=3) (~14 months old). (**i**) Ad libitum fed serum non-esterified fatty acid (NEFA) levels in aged control (n=9) and fTreg KO mice (n=10). (**j**) Serum resistin levels in ~14 month old fasted control and fTreg KO mice (n=4 pooled samples (2 mice per sample) per group). (**k**) Post-prandial glucose uptake in visceral adipose tissue of aged control (n=5) and fTreg KO mice (n=4). (**l**) Representative H&E staining of liver from ~14 month old control (n=3) and fTreg KO mice (n=5) (scale bar, 200 μM). (**m**) Hepatic triglyceride levels in ~14 month old control (n=5) and fTreg KO mice (n=3). (**n**) Fasting serum triglycerides in ~14 month old control (n=9) and fTreg KO mice (n=10). (**o**) fTregs, expressed as % of total $CD45.2^+$ cells, in control and IL2/anti-IL2 treated mice (n=3 mice per group). (**p**) Relative glucose uptake in VAT of 16 week old wild-type and IL2/anti-IL2 treated mice (n=4 mice per group). Data represents mean ± s.e.m. *p<0.05, **p<0.01, ***p<0.001, ****p<0.0001.

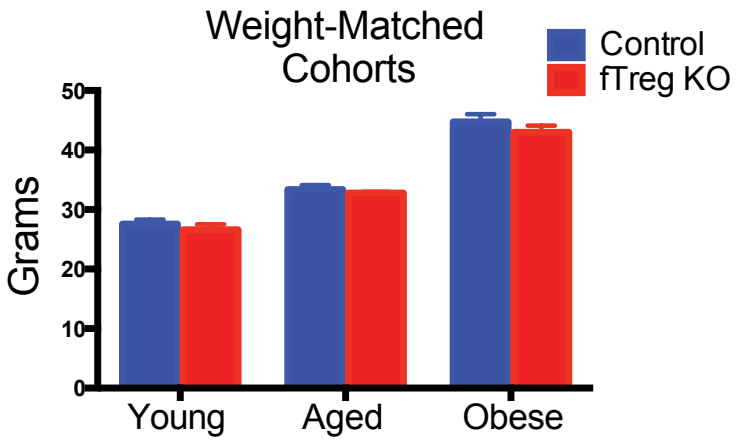

Figure 8. Body weights of weight-matched cohorts of control and fTreg KO young, aged, and obese mice. Body weights of fTreg KO and control male mice used in weight-matched metabolic studies in young (12 week old; control n=9; fTreg KO n=9), aged (36 week old; control, n=9 mice; fTreg KO, n=11 mice), and obese (DIO, 12 weeks of HFD starting at 12 weeks old; control n=10; fTreg KO n=10) settings.

seen in young or obese fTreg KO mice (Fig. 7d,f), which is consistent with the largely unchanged AIP of obese fTreg KO mice (Fig. 9).

Histologically, aged fTreg KO VAT depots appear similar to control mice, and inflammatory processes such as crowning are observed at comparable frequencies (Fig. 7g, data not shown). However, adipocytes from aged fTreg KO mice are smaller than those in control mice (fTreg KO 70% <5000 μm^2, control ~41% <5000 μm^2, Fig. 7h, Fig. 10), and serum non-esterified free fatty acid (NEFA) levels are reduced to almost half those of control mice; both indicators of improved insulin sensitivity (Fig. 7i). In addition, circulating levels of the adipokine resistin, which positively correlates with murine insulin resistance, are reduced in the aged fTreg KO mice (Fig. 7j)[29-30]. Furthermore, aged fTreg KO mice present with decreased hepatic steatosis, as determined histologically and by decreased fasting hepatic and serum triglyceride content (Fig. 7l-n). In combination, these findings suggest that the loss of fTregs in adipose tissue alleviates many of the indications of age-associated IR in mice, a primary clinical manifestation of metabolic aging.

To more directly associate fTregs with age-associated IR, we measured basal glucose uptake in adipose tissue *ex vivo*. Notably, VAT from fTreg KO mice took up almost twice the amount of glucose as control tissue (Fig. 7k). Conversely, expansion of fTregs in WT mice via treatment with IL-2/IL-2 mAb complex treatment[31] abrogates basal glucose uptake in VAT by ~50% (Fig. 7o,p). This inverse correlation between fTreg numbers and glucose uptake in

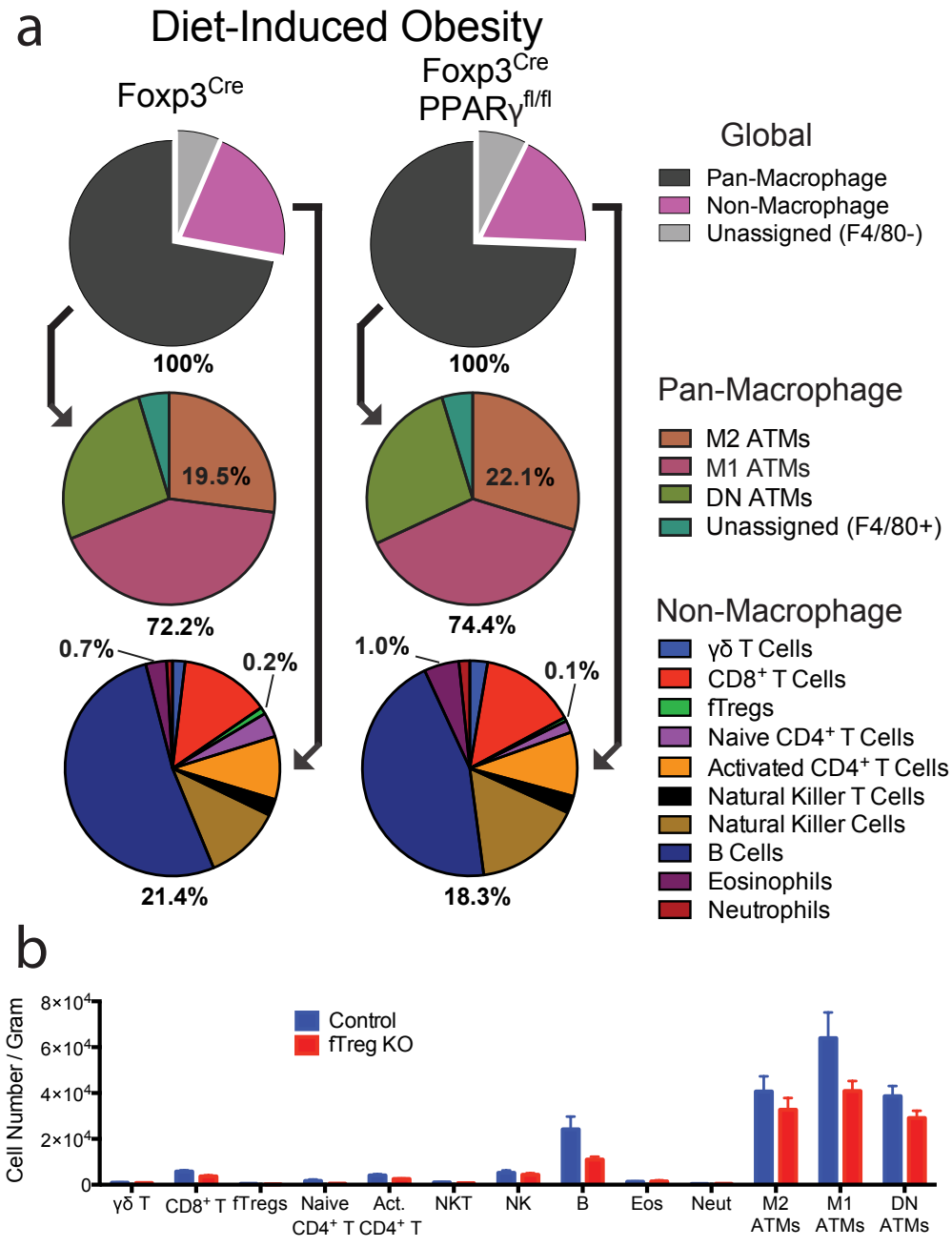

Figure 9. VAT AdipoImmune profiles of obese fTreg KO and control mice. (**a**) AdipoImmune profiles of obese (DIO, 16 weeks high fat diet started at 12 weeks of age) control (n=6 mice) and fTreg KO (n=8 mice) male mice depicting immune cell abundance, expressed as percentage of CD45.2+ cells. Entirety of immune compartment (top) is further divided into pan-macrophage (middle) and non-macrophage (bottom) pie charts. (**b**) Immune cell abundance between fTreg KO and control mice, expressed as cells per gram of VAT (n=9 mice per group). Data represents mean ± s.e.m.

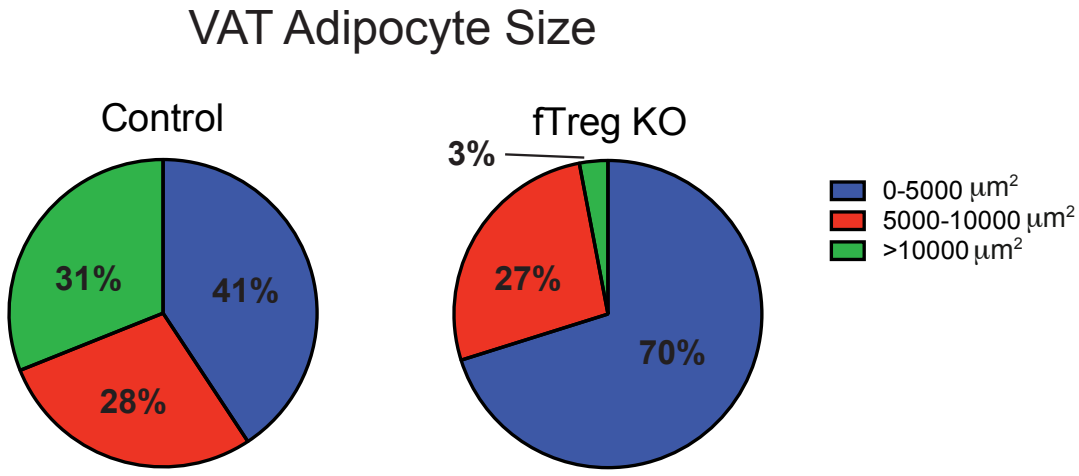

Figure 10. Frequency of small, medium, and large adipocytes in VAT of aged control and fTreg KO mice. Frequency of small (0-5000 μm^2), medium (5000-10,000 μm^2), and large (>10,000 μm^2) adipocytes in VAT of aged control and fTreg KO mice (n=3 mice per group, 850 adipocytes counted from control mice, 269 adipocytes counted from fTreg KO adipose).

adipose tissue supports a causal association between fTregs and IR during aging.

Our findings of an association between fTregs and age-associated IR and metabolic aging suggest that these cells are functionally distinct from splenic Tregs. To investigate this notion, we compared the transcriptomes of Tregs, as well as conventional $CD4^+$ T (Tconv) cells, isolated from VAT and spleen. Comparative analyses revealed that while certain canonical genes are similarly expressed (e.g. *Foxp3*, *Ctla4*, and *Tigit*), VAT and splenic Tregs have discrete expression signatures, consistent with the suggested functional distinction. In particular, *Pparg*, *Gata3*, and *Irf4* are selectively enriched in VAT but not splenic Tregs[32] (Fig. 11a). Furthermore, unbiased comparative gene expression analyses combined with hierarchical clustering defined extensive fat- and splenic-residence clusters (1142 genes and 1431 genes, respectively) relative to much smaller Pan-Treg Clusters 1 and 2 (56 and 162 genes, respectively). Transcriptionally, fTregs cluster more closely with fat Tconv cells than splenic Tregs (Fig. 12a), suggesting that the functional specification of fTregs is informed by their anatomical location within adipose tissue, as well as the expression of the Treg lineage-specifying transcription factor Foxp3[33,34]. We posited that the transcriptional differences between fTregs and splenic Tregs (found in the fTreg cluster of 1049 genes) may provide a therapeutic avenue to selectively manipulate fTreg populations. The IL-33 receptor ST2, which lies within the fTreg cluster, has been recently implicated in effector Treg

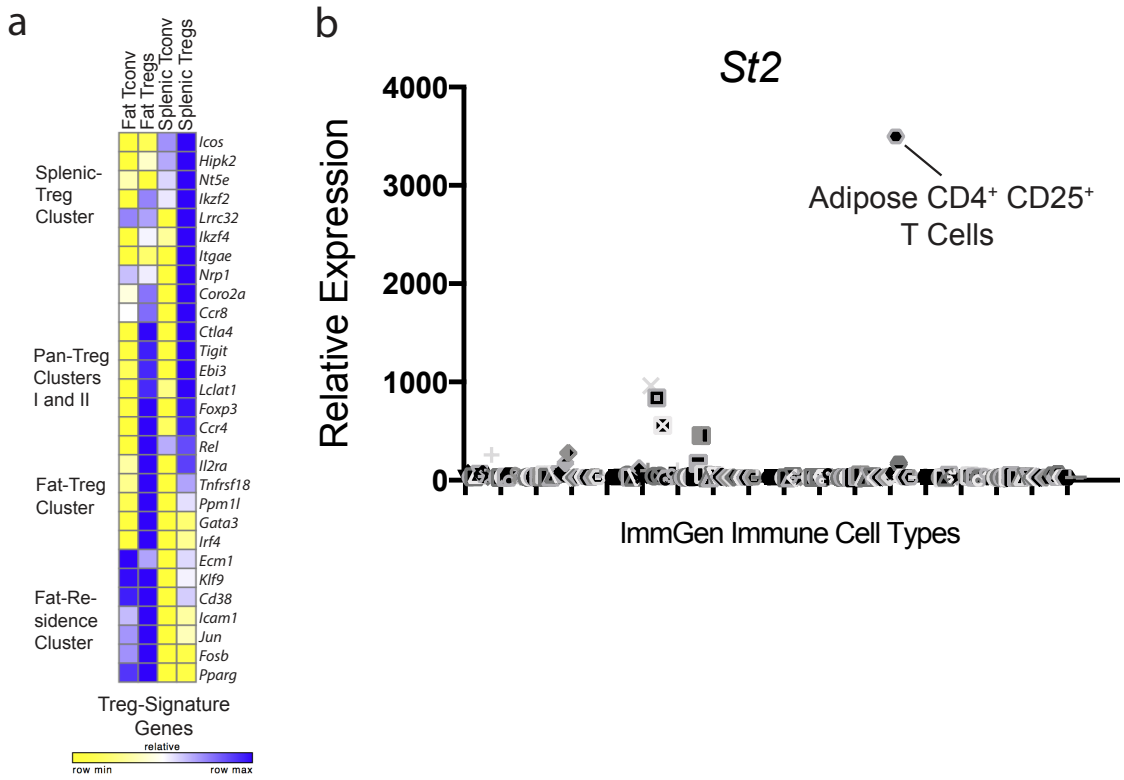

Figure 11. fTreg gene expression. (**a**) Expression of several canonical Treg genes across fat and splenic Tregs and fat and splenic Tconv cells. Cells were pooled from 3 and 4 mice before isolating RNA for subsequent RNA-Seq analysis. (**b**) Expression of ST2 across all hematopoietic cells catalogued in the ImmGen database. Position of adipose CD4^{+} CD25^{+} T cells is marked.

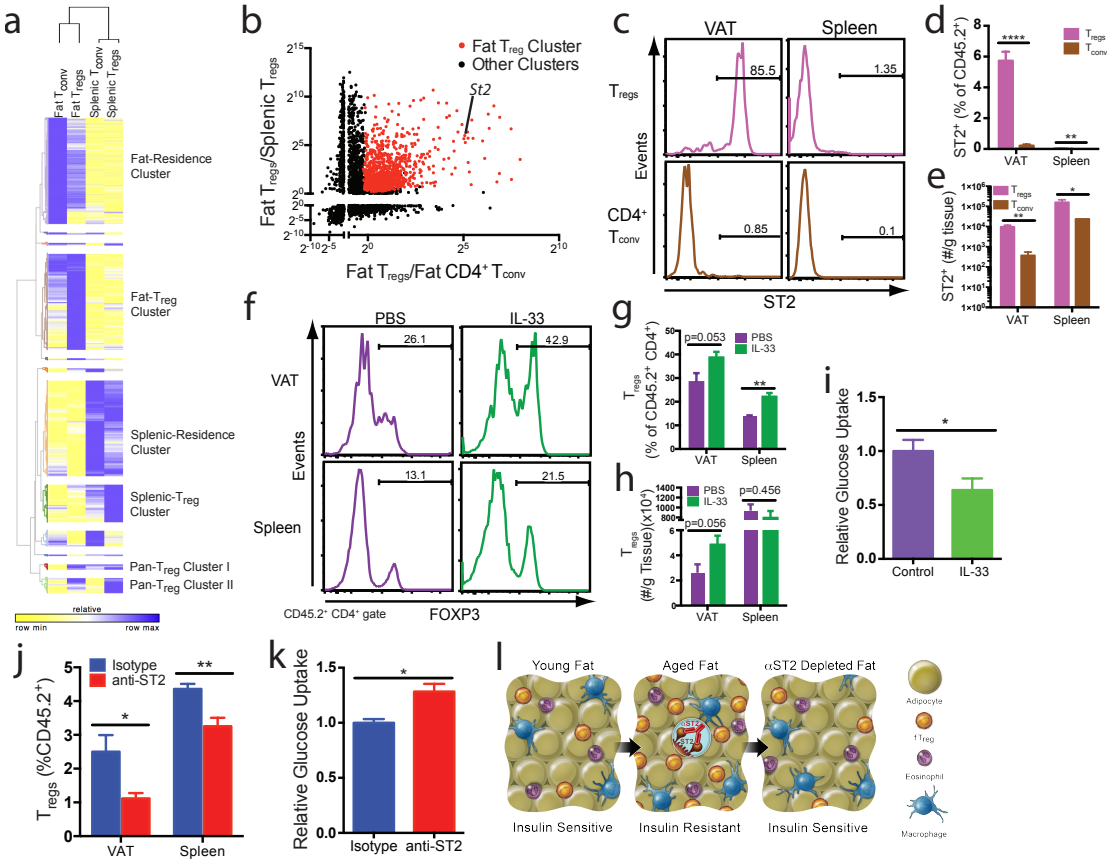

Figure 12. fTreg depletion improves adipose glucose uptake. (**a**) Hierarchical clustering of differentially expressed genes between fat Tregs and Tconv and splenic Tregs and Tconv cells,, and (**b**) Fold change in expression levels of differentially expressed genes across fat Tregs and Tconv and splenic Tregs and Tconv cells from Foxp3-Thy1.1 mice (47 weeks, cells pooled from 3 to 4 mice). Fat Treg cluster genes are labeled in red. Position of ST2 is marked. (**c**) Representative FACS analysis and (**d**) quantification of ST2 expression in CD4+ T cells from aged mice (45 weeks, n=5 mice). (**e**) Total number of ST2+ Tregs and Tconv cells per gram of tissue in VAT and spleen (n=5 mice). (**f**) FACS histograms and (**g**) quantification of Tregs (%Foxp3+ of CD45+ CD4+ population), and (**h**) cells per gram of tissue in VAT and spleen after IL-33 or PBS treatment (16 weeks, n=5 mice per group). (**i**) *Ex vivo* glucose uptake in VAT from wild type mice after control or IL-33 treatment (16 weeks, n=5 mice per group). (**j**) Quantification of fTregs and splenic Tregs (%Foxp3+ of CD45+ population) and (**k**) *ex vivo* insulin stimulated glucose uptake in VAT from wild type mice after anti-ST2 depleting antibody or isotype control treatment (~45 weeks old, n=4 mice per group). (**l**) Adipo-immune model of metabolic aging. Data represents mean ± s.e.m. *p<0.05, **p<0.01.

and in particular fTreg development[35,36]. Indeed, ST2 was ~60 and ~30 times more highly expressed in fTregs compared to splenic Tregs and fat Tconv cells, respectively, consistent with the ImmGen database (http://www.immgen.org), (Fig. 11b, Fig. 12b). Flow cytometry confirmed that ST2 is expressed on the cell surface of the majority of fTregs, but on relatively few fat Tconv, or splenic Tregs or Tconv cells (Fig. 12c,d). Furthermore, VAT has ~10x more $ST2^+$ fTregs than $ST2^+$ fat Tconv; a similar ratio is seen in the spleen (Fig. 12e).

To explore the therapeutic potential of the IL-33/ST2 signaling pathway, aged mice were initially injected with IL-33 (0.5 µg i.p. on days 0, 2, 4) to expand the fTreg population (Fig. 12f-h). In agreement with fTreg expansion driven by IL2/anti-IL2 treatment, mice injected with IL-33 display signs of IR (basal glucose uptake in VAT reduced to ~60% of control mice, Fig. 12i). In the converse approach, acute treatment with an anti-ST2 antibody (200 µg/mouse i.p. on days 0 and 2) is able to partially deplete fTregs (~50% reduction), with a smaller percentage reduction of splenic Tregs (Fig. 12j). Importantly, partial depletion of fTregs achieved with acute anti-ST2 treatment is sufficient to increase insulin-stimulated glucose uptake in VAT (~25% increase in glucose uptake compared to control treated mice, Fig. 12k). Furthermore, this increase in insulin sensitivity is achieved without any signs of Tconv cell activation associated with systemic Treg dysfunction (Fig. 13).

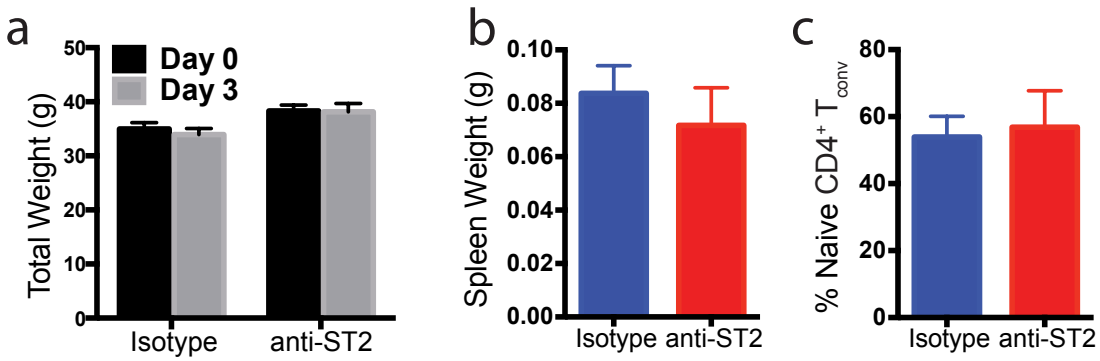

Figure 13. Depleting anti-ST2 antibody treatment does not promote T cell activation associated with systemic Treg-dysfunction. (**a**) Total weight before beginning course of anti-ST2 or isotype control antibodies (Day 0) and upon terminal analysis. Spleen weight (**b**) and percentage of splenic naive $CD4^+$ T cells as defined by $CD62^{hi}$ $CD44^{lo}$ relative to total splenic $CD45^+$ $CD4^+$ $CD25^-$ T cell population (**c**) of mice upon terminal analysis (Day 3, n=4 mice per group).

Taken together, our data provide evidence that distinct adipo-immune populations drive age- and obesity-associated IR. The findings that fTregs accumulate in mouse adipose tissue as a function of age and exacerbate the decline of adipose metabolic function associated with aging (Fig. 12l), complements the established role of M1 ATMs in the decline of adipose metabolic function in the setting of obesity. Thus, these studies showcase the ability of the immune compartment within adipose to drive key aspects of metabolic aging, in particular IR. Given the classical immune suppressive and anti-inflammatory nature of Tregs, we speculate that the chronic inflammatory processes that drive obesity-associated IR are likely not driving age-associated IR. Indeed, based on recent studies, it is possible that maintaining a certain degree of inflammation is beneficial for adipose tissue remodeling and its metabolic function[37], and the increased abundance of fTregs in the aged state may prevent beneficial inflammatory processes like adipose remodeling necessary for maintenance of adipose insulin sensitivity. Finally, our study suggests that selective targeting of fTregs might represent a new therapeutic avenue in the treatment of age-related diabetes, and more generally provides a proof-of-principle that different subtypes of Tregs can be targeted in a clinically achievable manner bringing us closer to the promise that the identification of Tregs heralded many years ago.

The contents and data presented in this chapter is adapted from a Letter which was published in 2015 in the journal *Nature* titled “Depletion of fat-resident Treg cells prevents age-associated insulin resistance.” The authorship of this Letter is: Sagar P. Bapat, Jae Myoung Suh, Sungsoon Fang, Sihao Liu, Yang Zhang, Albert Cheng, Carmen Zhou, Yuqiong Liang, Mathias LeBlanc, Christopher Liddle, Annette R. Atkins, Ruth T. Yu, Michael Downes, Ronald M. Evans and Ye Zheng.

CHAPTER 3: DISCUSSION FOLLOWING THE MAIN TEXT

NEXT STEPS AND FURTHER EXAMINATIONS

Our work shows for the first time that fTreg accumulation in adipose tissue drives age-associated IR. This finding creates space for further investigations into how fTregs are impacting adipose tissue to promote IR in the aged context.

In particular, we asked two questions that were of interest to us.

1) Do fTregs have a role in glucose homeostasis in the context of obesity?

A previous study has provided evidence suggestive of an insulin-sensitizing function for fTregs in the setting of obesity. In particular, using the same fTreg KO mice that we utilized in our work, the study provided evidence to show that the insulin-sensitizing effect of the FDA-approved PPARγ agonists called thiazolidinediones (TZDs) required fTregs (which are high expressors of PPARγ). Of note, that study did not compare the metabolic performance of fTreg KO and control mice head-to-head in the context of HFD-induced obesity. Our results in such head-to-head comparisons found no significant differences in their serum fasting glucose and insulin levels, GTTs, and ITTs (Fig. 7b,c,f). We also did not observe a difference in the AIPs of fTreg KO and control mice in the obese context (Fig. 9a,b). Additionally, we observed a marked decrease in fTreg numbers in obese control mice compared to young as well as aged control mice (Fig. 7a) further suggesting

that fTreg KO and control obese mice likely should not exhibit significant differences when testing for glucose homeostasis.

We nevertheless investigated the necessity of fTregs for the insulin-sensitizing function of TZDs in mice. We used two interventional schemes to introduce the TZD (which in our studies was rosiglitazone (Rosi)) - a therapeutic scheme and a prophylactic scheme. In the interventional scheme, we allowed fTreg KO and control mice to be on a HFD until the establishment of obesity and consequent IR and then introduced Rosi with the HFD (Fig. 14a). We conducted assays to determine relative levels of IR of the fTreg KO and control mice before and after introduction of Rosi, and found that the fTreg KO and control mice both had profound insulin-sensitization after introduction of Rosi (Fig. 14b-g). In the prophylactic scheme, we introduced Rosi at initiation of HFD and measured glucose homeostasis using HOMA-IR, ITTs, and GTTs of fTreg KO and control mice on HFD with Rosi or HFD alone (Fig. 14h). We again found clear beneficial effects of TZDs in the fTreg KO and control mice (Fig. 14h-l). Collectively the results from these two schema argue against an essential role of PPARγ^{+} fTregs in exerting the insulin-sensitizing function of TZDs *in vivo*. These results are consistent with earlier data from our lab indicating that adipocytes are likely the chief therapeutic target of TZDs[38]. Nevertheless, since we were able to observe a TZD-induced increase in fTregs, we wondered whether the increased fTreg enrichment came before or or after the beneficial effects of TZD treatment. We found that the insulin-

Figure 14. fTregs are dispensable for TZDs to exert their therapeutic insulin-sensitizing effect. (**a**) Scheme used for longitudinal interventional study of control and fTreg KO mice which indicates when certain particular assays were conducted and whose results are described in panels (**b-g**) where rosiglitazone (Rosi) was introduced in diet after firmly establishing obesity with high-fat diet (HFD) alone for 3 months (n=8 mice per group). (**b**) Cohort weights during course of study. Black arrow indicates time when Rosi was introduced into diet. (**c**) Homeostatic model assessment of insulin resistance (HOMA-IR). (**d-e**) GTT (**d**) and glucose excursions of GTT (**e**) described as Area Under Curve (AUC). (**f-g**) ITT (**f**) and bar-graph quantitation of relative serum glucose decrease during ITT (**g**) described as Area Above Curve (AAC). (**h**) Scheme used for parallel prophylactic study of control and fTreg KO mice whose results are described in panels (**i-l**) where mice were placed on HFD for 3 months or HFD with Rosi for 3 months (n=8 mice per group). (**i**) Cohort weights at end of study. (**j**) HOMA-IR. (**k-l**) GTT and ITT of control (**k**) or fTreg KO (**l**) mice fed HFD or HFD with Rosi. (**m**) Scheme used to temporal relationship of TZD-induced fTreg expansion and TZD-induced insulin-sensitization in wild-type mice whose results are described in panels (**n-q**) where mice were fed HFD or HFD with Rosi for up to 11 weeks (n=10 mice per group, 5 mice of each group were sacrificed at 5 weeks after diet introduction and remaining 5 mice were sacrificed at 11 weeks). (**n**) HOMA-IR at 4 weeks. (**o**) GTT at 5 weeks. (**p**) ITT at 5 weeks. (**q**) Relative fTreg enrichment of mice fed HFD with Rosi versus mice fed HFD alone at 5 weeks and 11 weeks on diet.

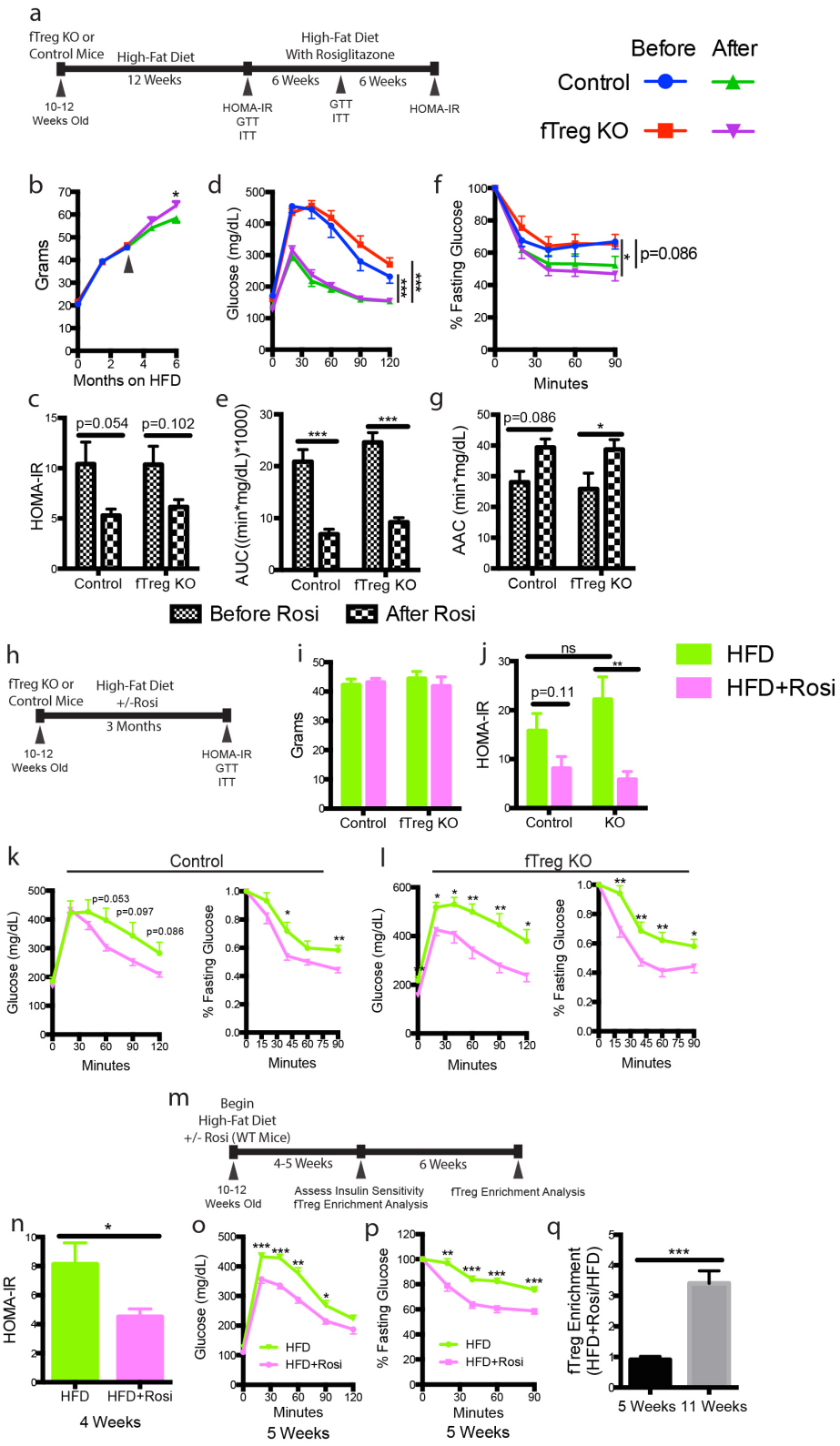
a
fTreg KO or Control Mice
High-Fat Diet
12 Weeks
High-Fat Diet With Rosiglitazone
6 Weeks
6 Weeks
10-12 Weeks Old
HOMA-IR GTT ITT
GTT ITT
HOMA-IR
Before After
Control
fTreg KO
b
Grams
Months on HFD
d
Glucose (mg/dL)
f
% Fasting Glucose
p=0.086
Minutes
c
HOMA-IR
p=0.054
p=0.102
Control fTreg KO
e
AUC ((min*mg/dL)*1000)
g
AAC (min*mg/dL)
p=0.086
Before Rosi
After Rosi
h
fTreg KO or Control Mice
High-Fat Diet +/-Rosi
3 Months
10-12 Weeks Old
HOMA-IR GTT ITT
i
Grams
Control fTreg KO
j
HOMA-IR
ns
p=0.11
Control KO
HFD
HFD+Rosi
k
Control
Glucose (mg/dL)
p=0.053
p=0.097
p=0.086
Minutes
% Fasting Glucose
l
fTreg KO
m
Begin High-Fat Diet +/- Rosi (WT Mice)
4-5 Weeks
6 Weeks
10-12 Weeks Old
Assess Insulin Sensitivity fTreg Enrichment Analysis
fTreg Enrichment Analysis
n
HOMA-IR
HFD HFD+Rosi
4 Weeks
o
Glucose (mg/dL)
HFD
HFD+Rosi
Minutes
5 Weeks
p
% Fasting Glucose
q
fTreg Enrichment (HFD+Rosi/HFD)
5 Weeks 11 Weeks

-sensitizing effect of TZDs preceded the TZD-induced fTreg enrichment in HFD-fed mice by a few weeks (Fig. 14m-q).

In our minds, these studies conclusively illustrate the non-essential role of fTregs for the insulin-sensitizing therapeutic mechanism of action of TZDs and further demonstrate that distinct immunopathologies undergird two distinct etiologies of IR - obesity-associated IR and aging-associated IR. But we know from experiences in the clinic that obesity and advancing age often coincide.

We thus wondered what role fTregs would have in aged and obese mice. Upon weight-matching a cohort of fTreg KO and control aged mice that were on lifelong normal chow, we introduced HFD and monitored the two groups' metabolic parameters. Interestingly, we found that the fTreg KO were initially more resistant to HFD-induced weight gain and other deleterious metabolic effects, but upon persistent HFD, the fTreg KO and control mice did not have have significantly different weights or performance on GTTs and ITTs (Fig. 15a-e). While we did not look more carefully at the changes in AIPs of the mice in this study, our previous results suggest that the fTreg KO mice underwent a change in their AIPs from what would be considered an aged AIP to an obese AIP, and thus the etiology of the underlying IR likely changed from an aged-associated IR to an obese-associated IR. Our work has shown that the fTreg KO mice are protective against specifically age-associated IR, and thus the fact that fTreg KO mice do not show any comparative benefit when placed on HFD when young or when aged is consistent with our model that

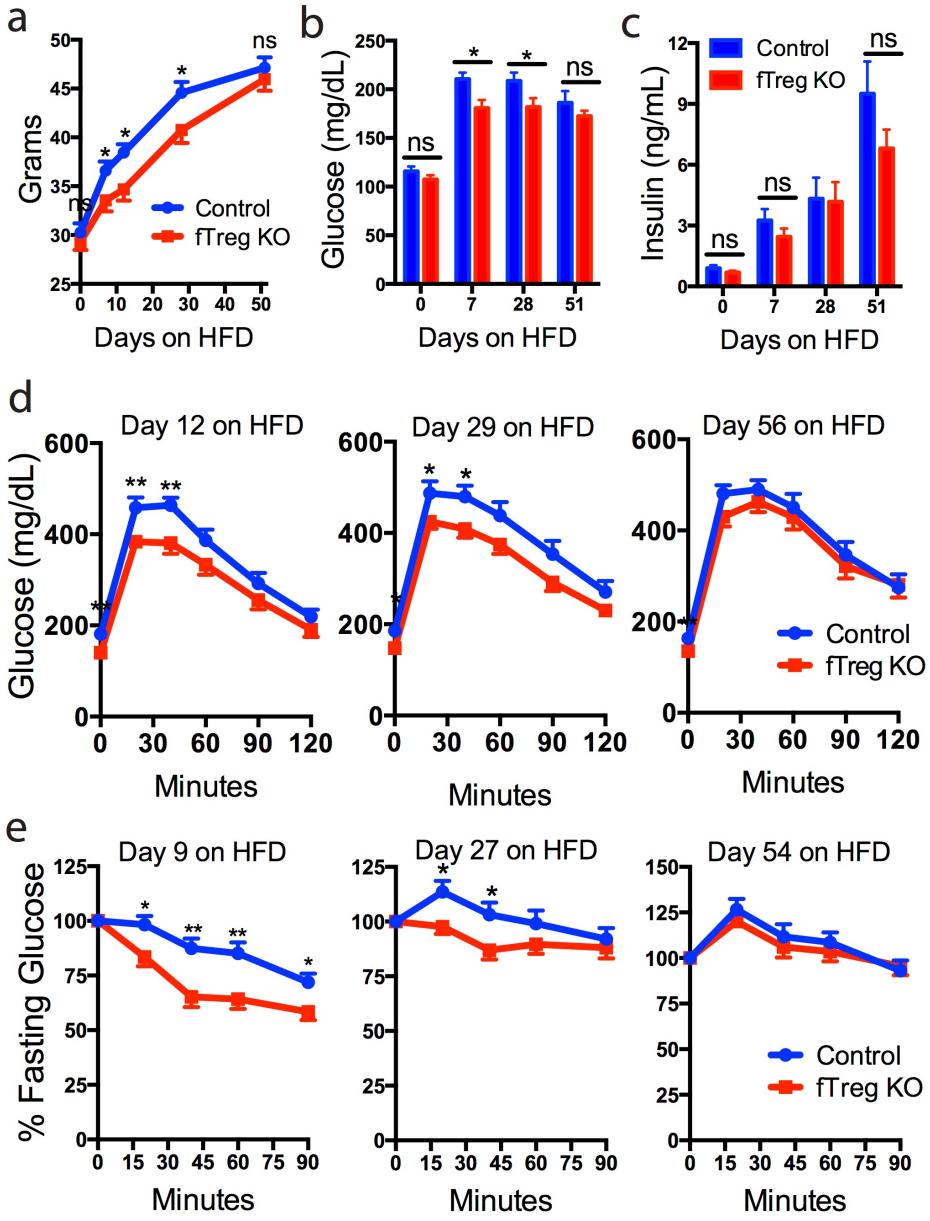

Figure 15. Aged fTreg KO mice are resistant to short-term, but not persistent, HFD-induced weight gain and insulin resistance. (**a-e**) Aged control and fTreg KO mice were placed on HFD and monitored throughout course of diet for weight (**a**), fasting glucose levels (**b**), fasting serum insulin levels (**c**), performance on GTT (**d**), and ITT (**e**). (Control, n=10; fTreg KO, n=11; Mice were aged 27-29 weeks and weight-matched before HFD was introduced.)

age-associated IR and obese-associated IR have two distinct immunopathological drivers.

2) How are fTregs affecting adipose tissue to cause progressive age-associated IR?

This question is particularly interesting when considering what is known about the mechanisms underlying obesity-associated IR. As mentioned earlier in the introduction, chronic inflammation is thought to be the chief link between obesity and the IR associated with obesity. More specifically, it is thought that obesity promotes increased inflammatory tone (e.g. increased inflammatory macrophage content, increased inflammatory cytokine concentrations, and decreased protective type-2 inflammation) which in turn promotes insulin resistance in obese adipocytes.

Intriguingly, Tregs are classically thought to be anti-inflammatory and immunosuppressive which normally decrease inflammatory tone, not induce increased chronic inflammation. While fTregs do have a significantly distinct gene expression signature compared to splenic Tregs, they do maintain high expression of genes important for classical Treg suppression including *Ctla4*[39], *Il2ra*[40], and the anti- inflammatory cytokine *Il10*[41] (Fig. 16a). We tested the ability of fTregs to functionally suppress conventional T cell activation and proliferation, and found that fTregs do maintain the canonical suppressive

functionality of all Tregs as measured by the *in vitro* suppression assay (Fig. 16b,c). This suggests that while fTregs may be exerting many effects on adipose tissue, one effect could be to decrease inflammatory tone.

Indeed, when we measured levels of TNFα by ELISA in adipose tissue of aged fTreg KO and control mice, we found that aged fTreg KO VAT has increased levels of TNFα suggesting that fTregs do indeed decrease inflammatory tone in aged adipose tissue (Fig. 17a). Upon a more global examination of gene expression changes of aged VAT in fTreg KO and control mice using RNA-Seq, we found a differential gene pattern indicative of an altered adipose tissue remodeling capacity in the fTreg KO mice compared to aged controls (Fig. 17b). In particular, we found increased expression of *Vegfa* in fTreg KO VAT (implicated in adipose remodeling and insulin sensitivity[42]) and decreased expression of extracellular matrix (ECM) genes (including all differentially expressed collagens (Fig. 17c), in particular, collagen VI implicated in adipose tissue rigidity[43], and the wound response gene Sparc) when compared to control tissue. Accompanying these changes, multiple proteases involved in ECM remodeling and angiogenesis (members of the ADAM, ADAMTS, MMP, and CELA families) were differentially expressed (Fig. 17d). These studies support a model in which fTregs decrease inflammatory tone to a level which impairs effective adipose tissue remodeling and angiogenesis and thus induces insulin resistance. Indeed, there is increasing

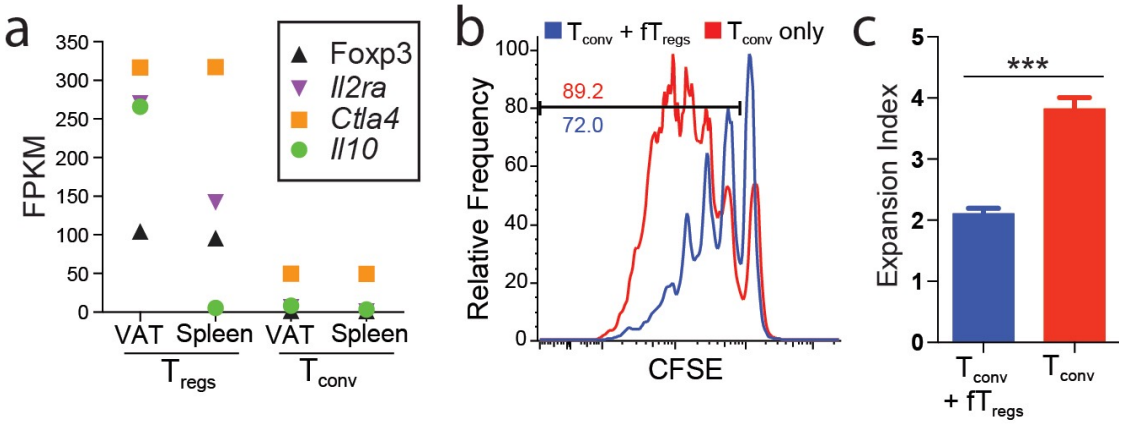

Figure 16. fTregs are immunosuppressive. (**a**) FPKM values of selected genes important for Treg identity and canonical suppressive function. (**b-c**) *In vitro* suppression assay of fTregs and splenic responder T cells (fTregs pooled from 9 retired breeders, added at 1:1 ratio with splenic responder T cells, conducted in technical triplicates). (**b**) Representative CFSE tracings of conventional T cells with or without fTregs. Gating indicates dividing cells. (**c**) Expansion index of Tconv cells.

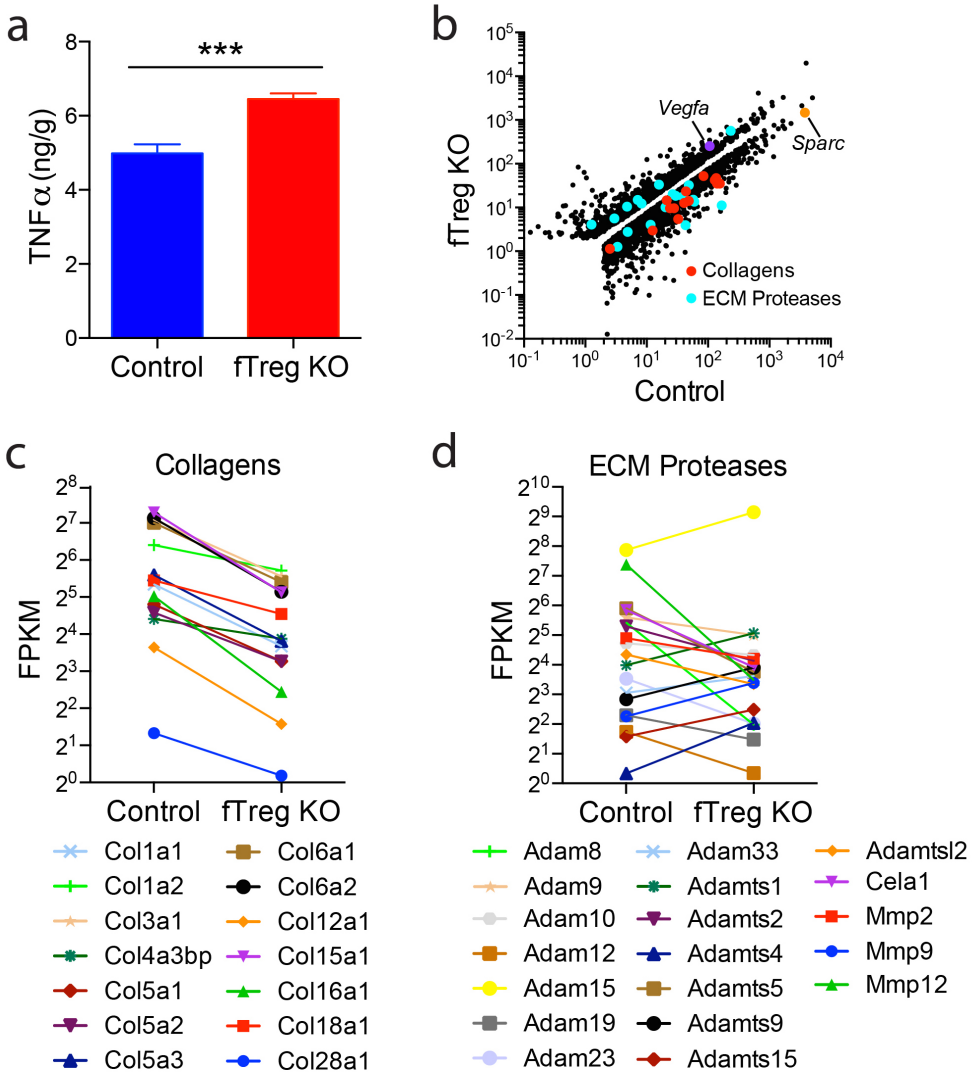

Figure 17. Increased TNFα levels and gene expression pattern of age fTreg KO adipose tissue is consistent with an improved adipose remodeling capacity. (**a**) TNFα levels quantified by enzyme linked immunosorbent assay (ELISA) of whole adipose lysate (~40 weeks old, n=6 per group). (**b**-**d**) FPKM values of all differentially expressed genes (**b**), differentially expressed collagens (**c**), and differentially expressed ECM proteases (**d**) in adipose tissue from aged fTreg KO and control mice (~40 weeks old, n=3 mice per group).

appreciation that maintaining a certain degree of inflammation is beneficial for adipose tissue remodeling and its metabolic function, and failure to preserve an optimal immune state in the aged adipose tissue may directly contribute to metabolic disorders such as IR and age-associated diabetes. Coupled with the known knowledge that too much inflammation is the causative agent of obesity-associated IR, our current work argues for a “sweet spot” for inflammatory tone to maintain insulin-sensitive adipose tissue. We would argue, that like in many other processes in biology, when it comes to inflammatory tone in adipose tissue, too much or too little yields pathological consequences.

Our findings described within the Main Text have also inspired other investigations into questions that have remained unanswered in the field of adipose biology for several years and are the subject of active inquiry in the lab. We are pursuing two areas of research that stem off of the central observation that fTregs seem to specifically enrich only in one particular WAT, the male epididymal white adipose tissue (eWAT, Figure 18). Strikingly, no other WAT in male mice seem to enrich with fTregs and all female WATs we have examined thus far also do not enrich with fTregs (Figure 19a,b).

Figure 18. Picture of epididymal WAT (eWAT), with the closely apposed testis attached.

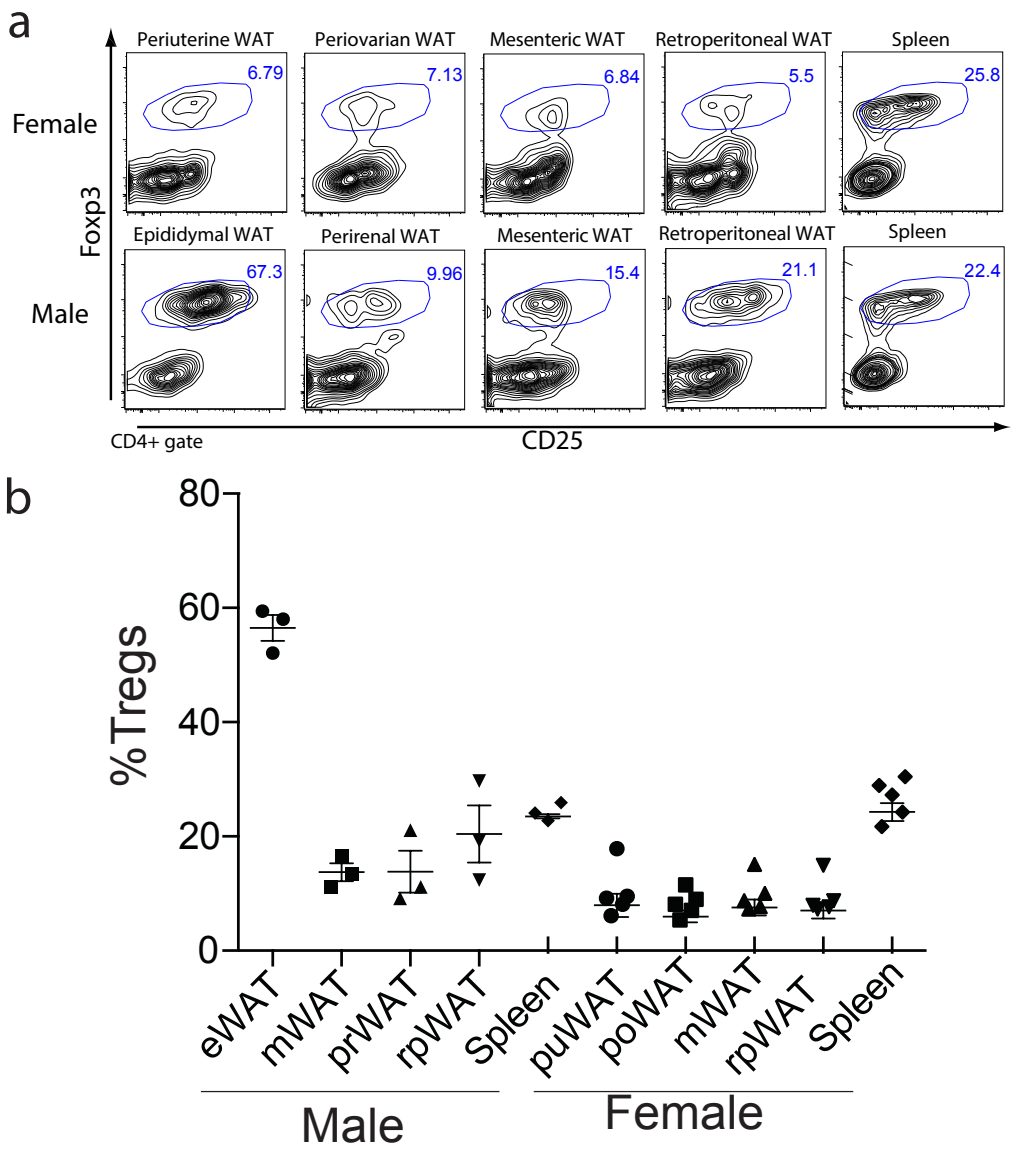

Figure 19. fTreg accumulation occurs predominantly in male eWAT. FACS analysis of Treg frequencies in spleen and stroma-vascular fractions of brown adipose and various white adipose tissue depots in both subcutaneous (inguinal) and visceral locations (epididymal, periuterine, periovarian, mesenteric, perirenal, retroperitoneal) from Foxp3-Thy1.1 reporter mice. Representative FACS plots (**a**) and quantitaive fTreg enrichment representation (**b**) of 8 month old male and female mice show predominant enrichment of fat-resident regulatory T cells (fTregs) in the male epididymal white adipose tissue. eWAT (epididymal white adipose tissue), mWAT (mesenteric white adipose tissue), prWAT (perirenal white adipose tissue), rpWAT (retroperitoneal white adipose tissue), puWAT (periuterine white adipose tissue), poWAT (periovarian white adipose tissue)

The questions we aim to answer include:

1) Given the generally protective role of SAT and pathogenic role of VAT in IR, what are the key cellular and molecular differences between SAT and VAT in male mice that drive these opposing roles?

It is well-appreciated in humans as well as in laboratory animals that not all adipose depots are equal. Different adipose depots have different anatomical shapes and locations and physiological functions. In fact, brown adipose tissue has a well established role of physiological burning of energy whereas the white adipose tissue's chief role is to be a storage depot for energy to be later utilized in times of energy scarcity. But the functional differences extend further as different WATs - dermal, subcutaneous, and visceral (including peri-renal, mesenteric, and gonadal) - have marked differences in storage capacity, basal lipolytic and glucose uptake rates, sensitivity to insulin, gene expression, and predisposition to promote IR upon HFD[44].

From the several studies that have characterized the different adipose depots in humans and laboratory animals, one key fact has emerged - SAT is generally protective against IR whereas VAT is pathogenic. Along with this key difference, we know of many other differences between SATs and VATs. SAT and VAT have markedly different gene expression profiles. The adipogenic

potential of their SVFs are very different with SVFs of SAT more able to promote adipogenesis. Upon a cold-challenge, the SATs are able to undergo beige adipogenesis (adipocytes that burn energy to create heat) whereas VATs are less able to do so[45,46]. Based upon our findings, SAT and VAT have very different AIPs. Notably, fTregs accumulate in male eWAT (a particular VAT) but not SAT.

Because of the known association of SAT mass and function with protection against IR, there has been an effort to understand the differences between SAT and VAT in order to make VAT more subcutaneous in its function. As each adipose depot is a highly complex network of genetic, cellular, and molecular interactions encompassing several physiological systems, it is unlikely that the perturbation of just one factor will completely transition VAT to SAT. However, because of our ability to essentially abolish fTreg accumulation in male VAT, our finding that fTreg-deficiency promotes protection against IR, and the finding that fTregs comprise the chief immunological difference in the AIPs between VAT and SAT, we hypothesize that depletion of fTregs in VAT promotes certain SAT functionality. Whether the functions include a more similar gene expression signature to SAT, an increased ability to promote beige adipogenesis, or some other function is still under active investigation.

2) Given the clear increased susceptibility for IR in male mice compared to female mice, what are the key cellular and molecular differences in the VATs of male and female mice that promotes IR in males but not females?

A noted feature between male and female humans is the differential predispositions of males to accumulate fat in their visceral adipose depots (creating an apple shaped habitus) and for females to accumulate fat in their subcutaneous depots (promoting a pear shaped habitus)[47]. Paired with known epidemiological observations that pre-menopausal women tend to be protected against IR compared to similarly-aged men, the findings in mice that SAT is protective against IR compared to VAT make us wonder whether the adipose tissues of females are globally more SAT-like compared to the adipose tissues of males and whether sex hormones, the chief differentiating factors in male and female development, physiology, and behavior, could be driving these adipose tissue differences. In particular, we wonder if the specific accumulation of fTregs in male VAT but not any female WATs is due to androgen signaling and is possibly a causative player in making males more susceptible to IR.

Indeed, when we castrate male mice through surgery or chemically via the gonadotropin-releasing hormone (GnRH) antagonist Azaline B, we notice a marked decrease in fTreg accumulation in male eWAT (Figure 20a,b). Additionally, the previously reported and successfully replicated TZD-induced

expansion of fTregs is abrogated in castrated mice (Figure 20c,d) suggesting an upstream role of androgen signaling to PPARg activation. Of further interest, androgen receptor (AR) KO bone-marrow chimeric mice had a ~50% decrease in their fTreg accumulation when compared to control mice further suggesting a role for androgens and androgen signaling in driving fTreg development and accumulation (Figure 21). Of note, AR and Foxp3, master lineage transcription factor of Tregs, interact biochemically, and, importantly, the avidity of the interaction increases with testosterone suggesting that the interaction is physiologically relevant (Figure 22). We have yet to assess whether or not AR signaling is functioning in fTreg-intrinsic or non-intrinsic capacity to promote fTreg accumulation, but we anticipate that the study of *Foxp3*^{Cre} *AR*$^{fl/fl}$ mice will help us answer that question. Our hypothesis moving forward is that androgen signaling, either through direct action within Tregs or indirectly through signaling within some other cell type within adipose tissue, is required for productive fTreg development and accumulation. This does not rule out a possible inhibitory role of estrogens for fTreg development and accumulation or the role of another factor required for fTreg development and accumulation that has not yet been identified.

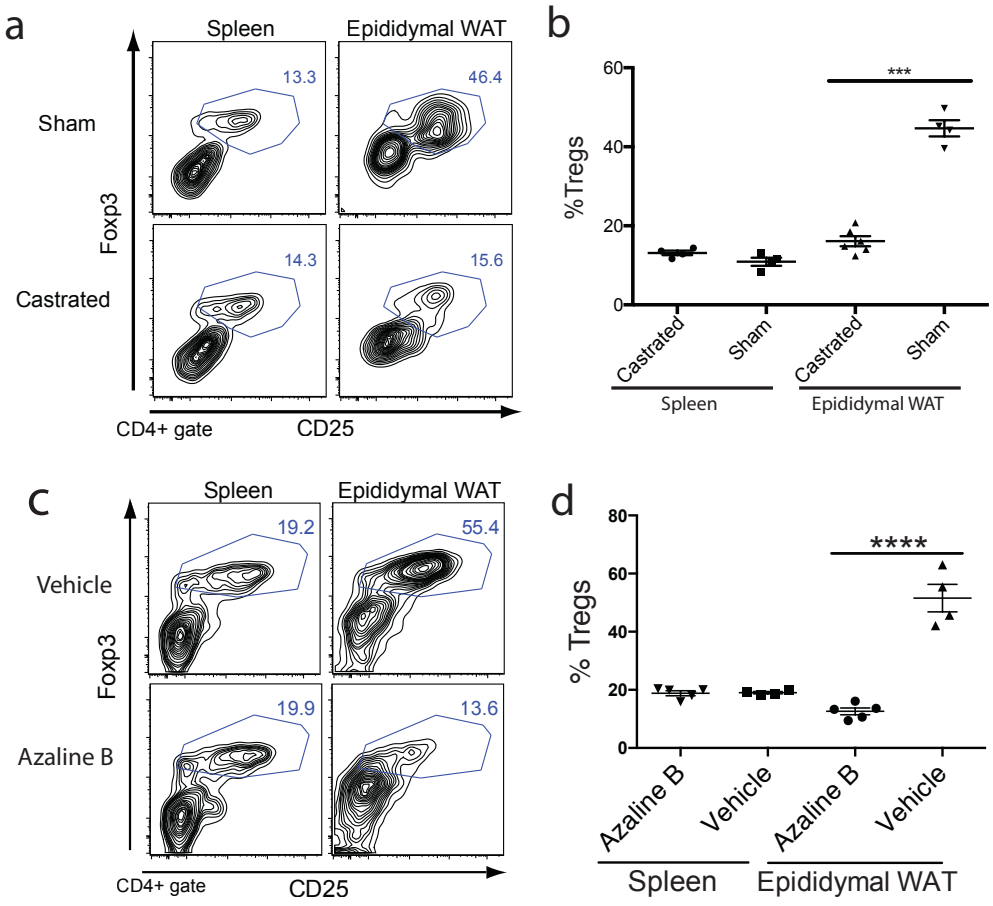

Figure 20. Male castration abrogates fTreg accumulation. (a,b) FACS analysis of spleen and epididymal white adipose tissue from wildtype C57BL/6 mice. Representative FACS plots (a) and quantitative fTreg enrichment representation (b) of 6 month old male mice show marked abrogation of fat-resident regulatory T cells (fTregs) in the male epididymal white adipose tissue of surgically castrated mice. Surgical castrations occured at 1 month of age. (c,d) FACS analysis of spleen and epididymal white adipose tissue from Foxp3-Thy1.1 mice fed HFD with TZD (Rosiglitazone). Representative FACS plots (c) and quantitative fTreg enrichment representation (d) show marked abrogation of TZD driven fTreg expansion in the male epididymal white adipose tissue of chemically castrated mice. Chemical castrations were conducted using the GnRH antagonist Azaline B, administered by intraperitoneal injection every 5 days for 11 weeks. **p<0.01, ***p<0.001,****p<0.0001

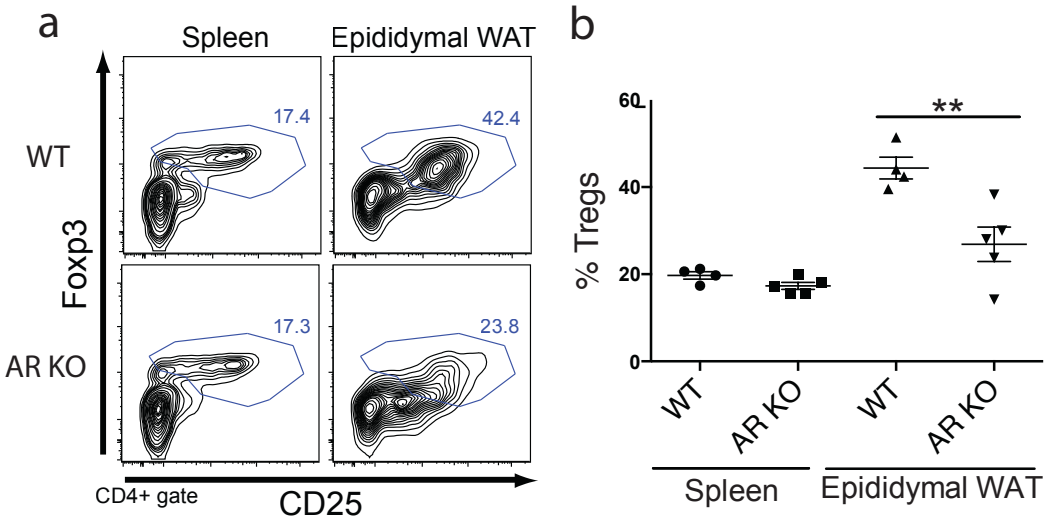

Figure 21. Androgen receptor deficient bone marrow chimeric mice have decreased accumulation of fTregs. Representative FACS plots (A) and quantitative fTreg enrichment representation (B) of bone marrow chimeric RAG -/- mice show marked abrogation of fat-resident regulatory T cells (fTregs) in the male epididymal white adipose tissue of mice with AR deficient bone marrow. **p<0.01

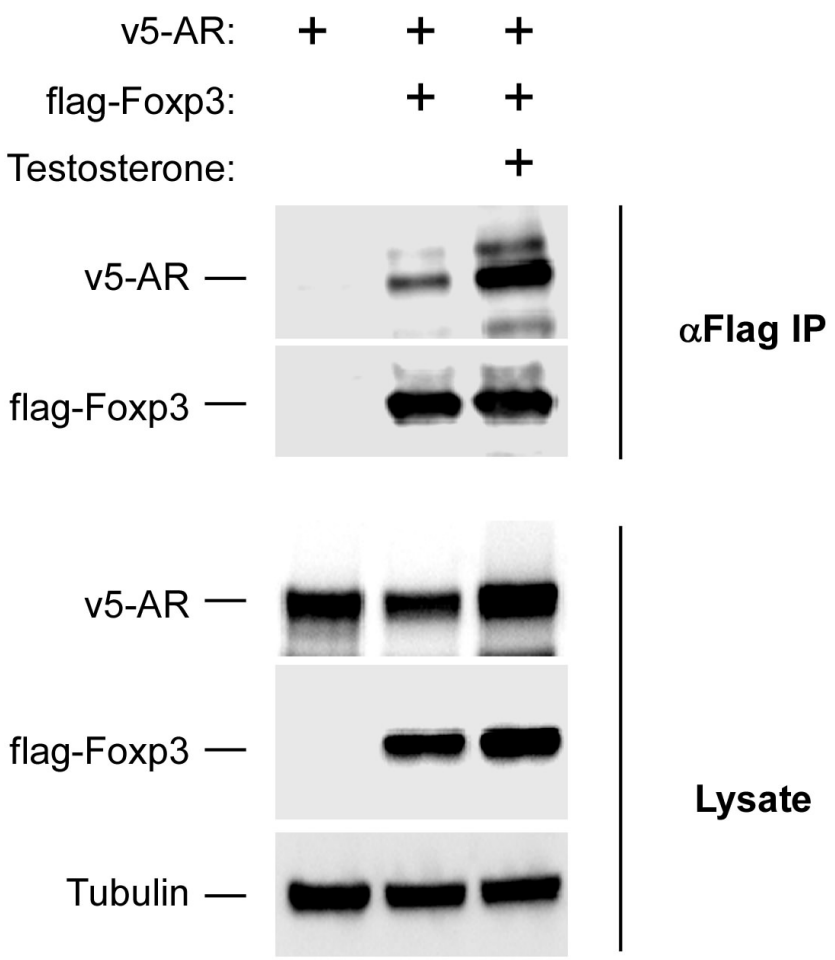

Figure 22. Androgen receptor interacts with Foxp3; Avidity of interaction increases with testosterone. Co-immunoprecipitation assay in HEK293 cells reveals association between AR and Foxp3. HEK293 cells were transfected with v5-AR and flag-Foxp3 or v5-AR alone. Doubly transfected cells were treated with 1uM testosterone overnight or ethanol.

The work described within the Main Text has laid the foundation for several future inquiries, only a small number of which have been described in this section, which could possibly create a window for elucidating previously unanswered and important physiological questions relating to aging, obesity, metabolic syndrome, and IR. As we have described in this thesis, our hope is that by using the tools and techniques familiar to both immunologists and molecular physiologists to study topics at the intersection of immunology and molecular physiology, the scientific community will be able to unveil some of the scientific mysteries that have thus far eluded us.

The contents and data presented in this chapter is adapted from a Letter which was published in 2015 in the journal *Nature* titled “Depletion of fat-resident Treg cells prevents age-associated insulin resistance.” The authorship of this Letter is: Sagar P. Bapat, Jae Myoung Suh, Sungsoon Fang, Sihao Liu, Yang Zhang, Albert Cheng, Carmen Zhou, Yuqiong Liang, Mathias LeBlanc, Christopher Liddle, Annette R. Atkins, Ruth T. Yu, Michael Downes, Ronald M. Evans and Ye Zheng.

METHODS

Mice. All mice were bred or housed in our specific pathogen-free facilities at The Salk Institute for Biological Studies or purchased from Taconic Biosciences. C57BL/6NTac and 129S6/SvEvTac mice were purchased from Taconic Biosciences for comparative adipo-immune profiling (AIP). Age-matched retired breeders were purchased for AIP of aged adipose, and DIO C57BL/6NTac mice were purchased for profiling of obese adipose. fTreg KO mice were generated by crossing B6.129(Cg)-Foxp3$^{tm4(YFP/cre)Ayr}$/J (41) and B6.129-Pparg^{tm2Rev}/J (48) mice. We utilized the Foxp3$^{Thy1.1}$ (49) reporter mice when isolating Tregs and conventional CD4^{+} T cells from spleen and fat for subsequent RNA-Seq analysis. Mice within The Salk Institute for Biological Studies received autoclaved normal chow (MI laboratory rodent diet 5001, Harlan Teklad) or autoclaved HFD (60 kcal% fat, Research Diets). All mice used for studies were male.

Adipo-immune profiling (AIP). Visceral (epididymal) and subcutaneous (inguinal) adipose depots were dissected from mice after 10mL PBS perfusion through left ventricle. Inguinal lymph nodes resident in inguinal adipose were removed. Adipose was minced into fine pieces (2-5mm^3) and digested in adipocyte isolation buffer (100mM HEPES pH7.4, 120mM NaCl, 50mM KCl, 5mM glucose, 1mM CaCl2, 1.5% BSA) containing 1mg/ml collagenase at

37°C with intermittent shaking for 1.5 hours. The suspension was then passed through a 100 μm mesh to remove undigested clumps and debri. The flowthrough was allowed to stand for 10 min to separate the floating adipocyte fraction and infranatant containing the stromal vascular fraction. The infranatant was removed while minimally disturbing the floating adipocyte fraction and centrifuged at 400g for 10 minutes. The pellet containing the stromal vascular fraction was washed once in 10mL RPMI. The resultant isolated cells were subjected to FACS analysis. The following antibodies were used to assemble the Adipo-immune Profile with the manufacturer preceding and clone number within parantheses: BioLegend - CD45.2 (104), CD44 (IM7), CD62L (MEL-14), TCRg/d (GL3), CD19 (6D5), CD25 (PC61), CD206 (C068C2), CD301 (LOM-14); eBioscience - CD3 (145-2C11), CD25 (PC61), CD4 (RM4-5), TCRb (H57-597), B220 (RA3-6B2), NK1.1 (PK136), CD49b (DX5), Foxp3 (FJK-16s), F4/80 (BM8), CD11c (N418), CD11b (M1/70); Tonbo biosciences - F4/80 (BM8.1), CD4 (RM4-5), CD44 (IM7), CD62L (MEL-14), Ly6G (RB6-8C5); BD Pharmingen - Siglec-F (E50-2440); BD Biosciences - CD8a (53-6.7). When analyzing myeloid cell populations, Fc blocking antibody (CD16/CD32, Tonbo biosciences, 2.4G2) was utilized. Cells were analyzed using the BD FACS Aria instrument and FlowJo software.

Body composition and adipocyte size analyses. Body composition was measured with an Echo MRI-100 body composition analyzer (Echo Medical

Systems). VAT (epididymal adipose) was dissected, and the wet weight was determined. Adipose tissues were fixed in 10% formalin, sectioned, and stained in hematoxylin and eosin. An adipocyte cross-sectional area was determined from photomicrographs of VAT using ImageJ.

***In vivo* metabolic phenotype analysis**. Real-time metabolic analyses were conducted in a Comprehensive Lab Animal Monitoring System (Columbus Instruments). CO_2 production, O_2 consumption, and ambulatory counts were determined for at least three consecutive days and nights after at least 24 h for adaptation before data recording.

Principal component analysis (PCA) of AIP. Non-macrophage immune cell populations, described as percent of the total $CD45.2^+$ immune compartment, were inputted into MetaboAnalyst 3.0 (http://www.metaboanalyst.ca/MetaboAnalyst/) for PCA. No normalizations, transformations, or scalings were implemented.

Glucose homeostasis studies. Fasting was induced for 6 h, except for GTTs, which were conducted after overnight fasting. Glucose (1-2 g/kg, i.p.) and insulin (0.5-1.0 U/kg, i.p.) was injected for GTTs and ITTs, respectively. Blood glucose was monitored using a Nova Max Plus glucometer.

Histological analyses. Sections (4 μm) of fixed tissues were stained with haematoxylin and eosin according to standard procedures. Histopathological scores were graded on blinded samples for severity and extent of inflammation and morphological changes by a pathologist.

Serum analyses. Blood was collected by tail bleeding or right atrial puncture. Non-esterified fatty acids (Wako) and triglycerides (Thermo) were measured using colorimetric methods. Serum insulin levels (Ultra Sensitive Insulin, Crystal Chem) were measured by ELISAs. Serum cytokine and metabolic hormone levels were analyzed by the Luminex Bio-Plex system using the Mouse Cytokine 23-Plex Panel and Diabetes Panel, respectively, as according to the manufacturer's instructions (Bio-Rad).

Core body temperature. Mice were single housed, and core body temperature was measured with a clinical rectal thermometer (Thermalert model TH-5; Physitemp) at 1:30PM. The probe was dipped in a room temperature lubricating glycerol before insertion.

***Ex vivo* 2-DG uptake assays.** Adipose was dissected from mouse, cut into small pieces with scissors, washed and incubated for 30 min with Krebs-Ringer Bicarbonate HEPES buffer (KRBH, 120 mM NaCl, 4 mM KH_2PO_4, 1 mM $MgSO_4$, 0.75 mM $CaCl_2$, 30 mM Hepes, 10 mM $NaHCO_3$, pH 7.4,

supplemented with 1% fatty-acid free BSA). For determination of exogenous insulin-stimulated 2-deoxy-D-glucose (2-DG) uptake, adipose was incubated in KRBH with 100-200nM insulin for 20 mins in 37 °C. Cold 2-DG and hot 2-DG-1,2-^{3}H(N) was added to incubated adipose such that the final concentration of cold 2-DG was 0.1 mM and final quantity of hot 2-DG-1,2-^{3}H(N) was 0.1 μCi (assuming total reaction volume ~400 uL). Adipose was further incubated 20 mins in 37 °C, then washed three times with PBS before being lysed by scintillation fluid. 2-DG uptake was determined by measuring scintillation counts normalized to adipose mass utilized for assay. Non-specific 2-DG uptake levels were determined by treating adipose with cytochalasin B (0.1 μM final concentration) before addition of cold and hot 2-DG.

IL-2-anti-IL-2 complex and IL-33 injections. IL-2-anti-IL-2 complexes were prepared by incubating 2 μg of murine IL-2 (Biolegend) with 10 μg of anti-IL-2 antibody (JES6.1, Bioxcell) in a total volume of 200 μL of PBS for 30 min at 37°C (amounts given per injection). Mice were injected i.p. three times (days 0,1, 2) and analyzed on day 8. For IL-33 expansion assays, mice were injected i.p. with 0.5 μg of recombinant murine IL-33 in PBS (R&D systems) three times (days 0, 2, 4) and analyzed on day 6. PBS was used for control injections.

RNA-Seq library generation. Total RNA was isolated from sorted cells using TRIzol reagent (Invitrogen) as per the manufacturer's instructions and treated with DNaseI (Qiagen) for 30 min at 22 °C. Sequencing libraries were prepared from 10-100 ng of total RNA using the TruSeq RNA sample preparation kit v2 (Illumina) according to the manufacturer's protocol. Briefly, mRNA was purified, fragmented and used for first- and second-strand cDNA synthesis followed by adenylation of 3′ ends. Samples were ligated to unique adaptors and subjected to PCR amplification. Libraries were then validated using the 2100 BioAnalyzer (Agilent), normalized and pooled for sequencing. RNA-Seq libraries prepared from two biological replicates for each experimental condition were sequenced on the Illumina HiSeq 2500 using barcoded multiplexing and a 100-bp read length.

High-throughput sequencing and analysis. Image analysis and base calling were done with Illumina CASAVA-1.8.2. This yielded a median of 29.9M usable reads per sample. Short read sequences were mapped to a UCSC mm9 reference sequence using the RNA-Seq aligner STAR[50]. Known splice junctions from mm9 were supplied to the aligner and de novo junction discovery was also permitted. Differential gene expression analysis, statistical testing and annotation were performed using Cuffdiff 2[51]. Transcript expression was calculated as gene-level relative abundance in fragments per kilobase of exon model per million mapped fragments and employed

correction for transcript abundance bias[52]. RNA-Seq results for genes of interest were also explored visually using the UCSC Genome Browser.

Hierarchical Clustering. Differentially expressed gene names and corresponding FPKM values across samples were inputted into GENE-E (Broad Institute) for hierarchical clustering analysis (implemented one minus pearson correlation for sample and gene distance metrics and the average linkage method) and visualization. Gene cluster names were created to describe the gene expression characteristics within each cluster (i.e. Fat-Residence Cluster refers to the gene cluster whose genes are expressed at greater levels in T cells residing in fat. Fat-Treg Cluster refers to the gene cluster whose genes are expressed highest in only the fTregs.)

In vitro suppression assay. fTregs were isolated from retired breeders that were treated with IL-2/anti-IL-2 complexes to expand fTreg numbers as written above. Stromal vascular fractions (SVFs) were isolated from visceral adipose tissues as described above, and fTregs were sorted from SVFs using the BD FACSAria instrument (Becton Dickinson), gating on $CD45.2^+$ $CD3^+$ $CD4^+$ $CD25^+$ cells. $CD45.1^+$ mice were sacrificed to isolate splenic responder T cells, which were purified by positive selection using CD4-specific Dynabeads (Invitrogen), followed by sorting on a BD FACSAria cell sorter, gating on $CD45.1^+$ $CD4^+$ $CD25^-$ $CD62L^{hi}$ $CD44^{lo}$ cells. Antigen-presenting cells were prepared from wild-type B6 splenocytes by T-cell depletion using Thy1-specific

MACS beads. Effector T cells (5×10^4 cells well^{-1}) were co-cultured with fTregs at the indicated ratio in the presence of irradiated (30 Gy) antigen-presenting cells (1×10^5 cells well^{-1}) in 96-well plates in complete RPMI1640 medium supplemented with 10% FBS and CD3 antibody (1 μg ml^{-1}). CFSE was added to monitor cell proliferation and expansion index which was acquired 96h later using the BD FACSAria instrument and analyzed with the FlowJo software package (Tree Star).

ST2 studies and anti-ST2 depleting antibody treatment. FACS antibody for ST2 was purchased from MD Bioproducts, clone DJ8. Mice were injected i.p. with 200 μg depleting anti-ST2 antibodies[53] (R&D systems, clone 245707) or isotype control (Bioxcell) twice (days 0, 2) and sacrificed for analysis on day 3.

Statistical analyses. Statistical analyses were performed with Prism 6.0 (GraphPad). p values were calculated using two-tailed unpaired or paired Student's t test. When analyzing adipo-immune profiles, we utilized a false discovery rate approach to avoid the problem of an inflated false-positive rate due to the substantial number of hypothesis tests. Mice cohort size was designed to be sufficient to enable statistical significance to be accurately determined. When applicable, mice were randomly assigned to treatment or control groups. No animals were excluded from the statistical analysis, with the exception of exclusions due to technical errors by investigators, and the investigators were not blinded in the studies. Appropriate statistical analyses

were applied, assuming a normal sample distribution, as specified in the figure legends. No estimate of variance was made between each group. All *in vivo* metabolic and glucose homeostasis experiments, *ex vivo* glucose uptake experiments, and adipo-immune profiling experiments were conducted with at least two independent cohorts. RNA-Seq experiments, Luminex profiling, and histological analyses were conducted using multiple biological samples (as indicated in figure legends) from indicated cohorts.

The contents and data presented in this chapter is adapted from a Letter which was published in 2015 in the journal *Nature* titled “Depletion of fat-resident Treg cells prevents age-associated insulin resistance.” The authorship of this Letter is: Sagar P. Bapat, Jae Myoung Suh, Sungsoon Fang, Sihao Liu, Yang Zhang, Albert Cheng, Carmen Zhou, Yuqiong Liang, Mathias LeBlanc, Christopher Liddle, Annette R. Atkins, Ruth T. Yu, Michael Downes, Ronald M. Evans and Ye Zheng.

REFERENCES

1. Ferrante, A. W., Jr. Macrophages, fat, and the emergence of immunometabolism. *J Clin Invest* **123,** 4992–4993 (2013).

2. Lumeng, C. N. & Saltiel, A. R. Inflammatory links between obesity and metabolic disease. *J Clin Invest* **121,** 2111–2117 (2011).

3. Mathis, D. Immunological Goings-on in Visceral Adipose Tissue. *Cell Metab* **17,** 851–859 (2013).

4. Osborn, O. & Olefsky, J. M. The cellular and signaling networks linking the immune system and metabolism in disease. *Nat Med* **18,** 363–374 (2012).

5. Weisberg, S. P., McCann, D., Desai, M., Rosenbaum, M., Leibel, R. L., & Ferrante Jr., A. W. Obesity is associated with macrophage accumulation in adipose tissue. *J Clin Invest* **112,** 1796–1808 (2003).

6. Xu, H., Barnes, G. T., Yang, Q., Tan, G., Yang, D., Chou, C. J., Sole, J., Nichols, A., Ross, J. S., Tartaglia, L. A., & Chen, H. Chronic inflammation in fat plays a crucial role in the development of obesity-related insulin resistance. *J Clin Invest* **112,** 1821–1830 (2003).

7. CDC. National Diabetes Statistics Report, 2014. 1–12 (2015).

8. The Finnish Diabetes Prevention Study Group. The Finnish Diabetes Prevention Study (DPS). Diabetes Care **26,** 3230-3236 (2003).

9. Diabetes Prevention Program Research Group. Reduction in the Incidence of Type 2 Diabetes with Lifestyle Intervention of Metformin. The New England Journal of Medicine **346,** 393–403 (2002).

10. Butryn, M. L., Webb, V. & Wadden, T. A. Behavioral Treatment of Obesity. *Psychiatric Clinics of North America* **34,** 841–859 (2011).

11. Curioni, C. C. & Lourenço, P. M. Long-term weight loss after diet and exercise: a systematic review. *Int J Obes Relat Metab Disord* **29,** 1168–1174 (2005).

12. Wadden, T. A., Butryn, M. L. & Wilson, C. Lifestyle Modification for the Management of Obesity. *Gastroenterology* **132,** 2226–2238 (2007).

13. Leal, J., Gray, A. M. & Clarke, P. M. Development of life-expectancy tables for people with type 2 diabetes. *European Heart Journal* **30,** 834–839 (2008).

14. Hotamisligil, G. S., Shargill, N. S., & Spiegelman, B. M., Adipose expression of tumor necrosis factor-alpha: direct role in obesity-linked insulin resistance. Science **259,** 87-91 (1993)

15. Uysal, K. T., Wiesbrock, S. M., Marino, M. W., & Hotamisligil, G. S. Protection from obesity-induced insulin resistance in mice lacking TNF-α function. Nature **389,** 610-614 (1997).

16. Hirosumi, J., Tuncman, G., Chang, L., Görgün, C., Uysal, K. T., Maeda, K., Karin, M., Hotamisligil, G. S. A central role for JNK in obesity and insulin resistance. Nature **420,** 333-336 (2002).

17. Xu, H., Barnes, G. T., Yang, Q., Tan, G., Yang, D., Chou, C. J., Sole, J., Nichols, A., Ross, J. S., Tartaglia, L. A., & Chen, H. Chronic inflammation in fat plays a crucial role in the development of obesity-related insulin resistance. *J Clin Invest* **112,** 1821–1830 (2003).

18. Lumeng, C. N., Bodzin, J. L. & Saltiel, A. R. Obesity induces a phenotypic switch in adipose tissue macrophage polarization. *J Clin Invest* **117,** 175–184 (2007).

19. Olefsky, J. M. & Glass, C. K. Macrophages, Inflammation, and Insulin Resistance. *Annu. Rev. Physiol.* **72,** 219–246 (2010).

20. Wu, D., Molofsky, A. B., Liang, H., Ricardo-Gonzalez, R. R., Jouihan, H. A., Bando, J. K., Chawla, A., & Locksley, R. M. Eosinophils sustain adipose alternatively activated macrophages associated with glucose homeostasis. *Science* **332,** 243–247 (2011).

21. Qiu, Y., Nguyen, K. D., Odegaard, J. I., Cui, X., Tian, X., Locksley, R. M., Palmiter, R. D., & Chawla, A. Eosinophils and Type 2 Cytokine Signaling in Macrophages Orchestrate Development of Functional Beige Fat. *Cell* **157,** 1292–1308 (2014).

22. Rao, R. R., Long, J. Z., White, J. P., Svensson, K. J., Lou, J., Lokurkar, I., Jedrychowski, M. P., Ruas, J. L., Wrann, C. D., Lo, J. C., Camera, D. M., Lachey, J., Gygi, S., Seehra, J., Hawley, J. A., & Spiegelman, B. M. Meteorin-like Is a Hormone that Regulates Immune-Adipose Interactions to Increase Beige Fat Thermogenesis. *Cell* **157,** 1279–1291 (2014).

23. Odegaard, J. I., Ricardo-Gonzalez, R. R., Goforth, M. H., Morel, C. R., Subramanian, V., Mukundan, L., Red Eagle, A., Vats, D., Brombacher, F., Ferrante, A. W., & Chawla, A. Macrophage-specific PPARgamma controls alternative activation and improves insulin resistance. *Nature* **447,** 1116–1120 (2007).

24. Fujisaka, S., Usui, I., Bukhari, A., Ikutani, M., Oya, T., Kanatani, Y., Tsuneyama, K., Nagai, Y., Takatsu, K., Urakaze, M., Kobayashi, M., & Tobe, K. Regulatory Mechanisms for Adipose Tissue M1 and M2 Macrophages in Diet-Induced Obese Mice. *Diabetes* **58,** 2574–2582 (2009).

25. Feuerer, M., Herrero, L., Cipolletta, D., Naaz, A., Wong, J., Nayer, A., Lee, J., Goldfine, A. B., Benoist, C., Shoelson, S., & Mathis, D. Lean, but not obese, fat is enriched for a unique population of regulatory T cells that affect metabolic parameters. *Nat Med* **15,** 930–939 (2009).

26. Lumeng, C. N., Liu, J., Geletka, L., Delaney, C., Delproposto, J., Desai, A., Oatmen, K., Martinez-Santibanez, G., Julius, A., Garg, S., & Yung, R. L. Aging Is Associated with an Increase in T Cells and Inflammatory Macrophages in Visceral Adipose Tissue. *The Journal of Immunology* **187,** 6208–6216 (2011).

27. Cipolletta, D., Feuerer, M., Li, A., Kamei, N., Lee, J., Shoelson, S. E., Benoist, C., and Mathis, D. PPAR-γ is a major driver of the accumulation and phenotype of adipose tissue Treg cells. *Nature* (2012). doi:10.1038/nature11132

28. Houtkooper, R. H., Argmann, C., Houten, S. M., Cantó, C., Jeninga, E. H., Andreux, P. A., Thomas, C., Doenlen, R., Schoonjans, K., & Auwerx, J. The metabolic footprint of aging in mice. *Sci. Rep.* **1,** (2011).

29. Steppan, C. M., Bailey, S. T., Bhat, S., Brown, E. J., Banerjee, R. R., Wright, C. M., Patel, H. R., Ahima, R. S., & Lazar, M. A. The hormone resistin links obesity to diabetes. *Nature* **409,** 307–312 (2001).

30. Schwartz, D. R. & Lazar, M. A. Human resistin: found in translation from mouse to man. *Trends Endocrinol Metab* **22,** 259–265 (2011).

31. Webster, K. E., Walters, S., Kohler, R. E., Mrkvan, T., Boyman, O., Surh, C. D., Grey, S. T., & Sprent, J. In vivo expansion of T reg cells with IL-2-mAb complexes: induction of resistance to EAE and long-term acceptance of islet allografts without immunosuppression. *J Exp Med* **206,** 751–760 (2009).

32. Feuerer, M., Hill, J. A., Kretschmer, K., Boehmer, H., Mathis, D., & Benoist, C. Genomic definition of multiple ex vivo regulatory T cell subphenotypes. *PNAS* **107,** 5919–5924 (2010).

33. Josefowicz, S. Z., Lu, L.-F. & Rudensky, A. Y. Regulatory T cells: mechanisms of differentiation and function. *Annu Rev Immunol* **30,** 531–564 (2012).

34. Ohkura, N., Kitagawa, Y. & Sakaguchi, S. Development and Maintenance of Regulatory T cells. *Immunity* **38,** 414–423 (2013).

35. Vasanthakumar, A., Moro, K., Xin, A., Liao, Y., Gloury, R., Kawamoto, S., Fagarasan, S., Mielke, L. A., Afshar-Sterle, S., Masters, S. L., Nakae, S., Saito, H., Wentworth, J. M., Li, P., Liao, W., Leonard, W. J., Smyth, G. K., Shi, W., Nutt, S. L., Koyasu, S., & Kallies, A. The transcriptional regulators IRF4, BATF and IL-33 orchestrate development and maintenance of adipose tissue–resident regulatory T cells. *Nat Immunol* 1–12 (2015). doi:10.1038/ni.3085

36. Schiering, C., Krausgruber, T., Chomka, A., Fröhlich, A., Adelmann, K., Wohlfert, E. A., Pott, J., Griseri, T., Bollrath, J., Hegazy, A. N., Harrison, O. J., Owens, B. M. J., Löhning, M., Belkaid, Y., Fallon, P. G., & Powrie, F. The alarmin IL-33 promotes regulatory T-cell function in the intestine. *Nature* **513,** 564–568 (2014).

37. Asterholm, I. W., Tao, C., Morley, T. S., Wang, Q. A., Delgado-Lopez, F., Wang, Z. V., & Scherer, P. E. Adipocyte Inflammation Is Essential for Healthy Adipose Tissue Expansion and Remodeling. *Cell Metab* **20,** 103–118 (2014).

38. Sugii, S., Olson, P., Sears, D. D., Saberi, M., Atkins, A. R., Barish, G. D., Hong, S.-H., Castro, G. L., Yin, Y.-Q., Nelson, M. C., Hsiao, G., Greaves, D. R., Downes, M., Yu, R. T., Olefsky, J. M., & Evans, R. E. PPARgamma activation in adipocytes is sufficient for systemic insulin sensitization. *PNAS* **106,** 22504–22509 (2009).

39. Wing, K., Onishi, Y., Prieto-Martin, P., Yamaguchi, T., Miyara, M., Fehervari, Z., Nomura, T., Sakaguchi, S. CTLA-4 Control over Foxp3^{+} Regulatory T Cell Function. *Science* **322,** 271-275 (2008).

40. Fontenot J. D., Rasmussen J. P., Gavin M. A., & Rudensky A. Y. A function for interleukin 2 in Foxp3-expressing regulatory T cells. *Nat Immunol* **6,** 1142-1151 (2005).

41. Rubtsov, Y. P., Rasmussen, J. P., Chi, E. Y., Fontenot, J., Castelli, L., Ye, X., Treuting, P., Siewe, L., Roers, A., Henderson Jr., W. R., Muller, W., & Rudensky, A. Y. Regulatory T Cell-Derived Interleukin-10 Limits Inflammation at Environmental Interfaces. *Immunity* **28,** 546–558 (2008).

42. Sun K., Asterholm I. W., Kusminski C. M., Bueno A. C., Wang Z. V., Pollard J. W., Brekken R. A., & Scherer P. E.. Dichotomous effects of VEGF-A on adipose tissue dysfunction. *PNAS* **109,** 5874-5879 (2012).

43. Khan T., Muise E. S., Iyengar P., Wang Z. V., Chandalia M., Abate N., Zhang B. B., Bonaldo P., Chua S., & Scherer P. E.. Metabolic dysregulation and adipose tissue fibrosis: role of collagen VI. *Mol Cell Biol* **29,** 1575-1591 (2009).

44. Tchkonia, T., Thomou, T., Zhu, Y., Karagiannides, I., Pothoulakis, C., Jensen, M. D., & Kirkland, J. L. Mechanisms and Metabolic Implications of Regional Differences among Fat Depots. *Cell Metab* **17,** 644–656 (2013).

45. Lee, M.-W., Odegaard, J. I., Mukundan, L., Qiu, Y., Molofsky, A. B., Nussbaum, J. C., Yun, K., Locksley, R. M., & Chawla, A. Activated Type 2 Innate Lymphoid Cells Regulate Beige Fat Biogenesis. *Cell* 1–14 (2014).

46. Rao, R. R., Long, J. Z., White, J. P., Svensson, K. J., Lou, J., Lokurkar, I., Jedrychowski, M. P., Ruas, J. L., Wrann, C. D., Lo, J. C., Camera, D. M., Lachey, J., Gygi, S., Seehra, J., Hawley, J. A., & Spiegelman, B. M. Meteorin-like Is a Hormone that Regulates Immune-Adipose Interactions to Increase Beige Fat Thermogenesis. *Cell* **157,** 1279–1291 (2014).

47. Wajchenberg, B.L. Subcutaneous and Visceral Adipose Tissue: Their Relation to the Metabolic Syndrome. *Endocrine Reviews* **21,** 697–738 (2000).

48. He, W., Barak, Y., Hevener, A., Olson, P., Liao, D., Le, J., Nelson, M., Ong, E., Olefsky, J. M., & Evans, R. M. Adipose-specific peroxisome proliferator-activated receptor gamma knockout causes insulin resistance in fat and liver but not in muscle. *PNAS* **100,** 15712–15717 (2003).

49. Liston, A., Nutsch, K. M., Farr, A. G., Lund, J. L., Jeffery P. Rasmussen†, Koni, P. A., & Rudensky, A. Y. Differentiation of regulatory Foxp3+ T cells in the thyme cortex. *PNAS* **105**, 11903–11908 (2008).

50. Dobin, A., Davis, C. A., Schlesinger, F., Drenkow, J., Zaleski, C., Jha, S., Batut, P., Chaisson, M., & Gingeras, T. R. STAR: ultrafast universal RNA-seq aligner. *Bioinformatics* **29,** 15–21 (2012).

51. Trapnell, C., Hendrickson, D. G., Sauvageau, M., Goff, L., Rinn, J. L., & Pachter, L. Differential analysis of gene regulation at transcript resolution with RNA-seq. *Nat Biotechnol* **31,** 46–53 (2012).

52. Roberts, A., Pimentel, H., Trapnell, C. & Pachter, L. Identification of novel transcripts in annotated genomes using RNA-Seq. *Bioinformatics* **27,** 2325–2329 (2011).

53. Monticelli, L. A., Sonnenberg, G. F., Abt, M. C., Alenghat, T., Ziegler, C. G. K., Doering, T. A., Angelosanto, J. M., Laidlaw, B. J., Yang, C. Y., Sathaliyawala, T., Kubota, M., Turner, D., Diamond, J. M., Goldrath, A. W., Farber, D. L., Collman, R. G., Wherry, E. J., & Artis, D. Innate lymphoid cells promote lung-tissue homeostasis after infection with influenza virus. *Nat Immunol* **12,** 1045–1054 (2011).